EFFECT OF WHEEL SLIP IN MODELING AND CONTROL OF WHEELED MOBILE ROBOTS: APPLICATIONS TO FORMATION CONTROL AND PURSUIT-EVASION PROBLEMS

By

Yu Tian

Dissertation

Submitted to the Faculty of the

Graduate School of Vanderbilt University

in partial fulfillment of the requirements

for the degree of

DOCTOR OF PHILOSOPHY

in

Mechanical Engineering

August, 2010

Nashville, Tennessee

Approved:

Professor Nilanjan Sarkar

Professor Akram Aldroubi

Professor Carol A. Rubin

Professor Robert J. Webster

Professor D. Mitchell Wilkes

ACKNOWLEDGEMENTS

The past five years has been a time of challenge for my research and a time of treasure for my life. I have been growing professionally in both research and personal career with the support of many people. I would like to take this chance to give my sincerest gratitude to those who have not only made this dissertation possible but also offered me support and help in the past few years.

This work would not have been possible without the financial support of Army Research Office grant, the Office of Naval Research grant or the Mechanical Engineering Department of Vanderbilt University.

Especially I would dedicate thanks from deep of my heart to Prof. Sarkar, my advisor and mentor, whose guidance, support, time and patience are invaluable. He has shown me, by example, how a good scientist should be.

My appreciation also goes to my Dissertation Committee, Prof. Rubin, Prof. Webster, Prof. Wilkes and Prof. Aldroubi for their times and interests in this dissertation. I must express my gratitude to my friends, Furui, Uttama, Vikash, Milind, Dr. Halder, Dr. Erol, Dr. Mallapragada, Dr. Sidek, Dr. Liu, Dr. Welch and Dr. Das, who together provide a friendly and conducive research environment.

Nobody has been more important to me in the pursuit of this work than the members of my family. I would like to thank my parents and my brother who gave me consistent support and motivation and taught me many things in my life. Most importantly, I wish to thank my wife, Di, who gives me unending love, support, inspiration and motivation.

TABLE OF CONTENTS

Page

LIST OF TABLES

Table Page

LIST OF FIGURES

CHAPTER I

INTRODUCTION

A Wheeled Mobile Robot (WMR) is a robotic mobile platform mounted with motors, sensors and a micro-processor or an onboard computer. Driven by the motors through the driving wheels, the WMR can move autonomously based on the sensory feedback and the control logic programmed into the onboard computer. Due to its mobility, sensing capability and autonomous decision without the involvement of human, WMRs have been extensively used in various applications such as in transportation, planetary exploration, intelligent surveillance, mining and military operations. Different kinds of WMR have different motion capabilities, which can be applied to different areas. Usually WMRs can be classified into nonholonomic WMRs and holonomic WMRs depending on their kinematic constraints. If the controllable degrees of freedom are equal to the total degrees of freedom then the robot is said to be holonomic. Holonomic robots are allowed to immediately move in any direction without the need to turn first. Because of such capability, holonomic robots are used in surveillance and soccer games where motion flexibility is required. However, note that, the holonomic robots require special wheels capable of moving omnidirectionally. Thus their versatile mobility comes at the expense of complex mechanical design and construction. On the other hand, if the controllable degrees of freedom are less than the total degrees of freedom then the robot is said to be nonholonomic. Not every path in the work space is achievable for a nonholonomic robot.

However such robots are widely used in exploration and transportation where motion flexibility is not a big concern. Nonholonomic mobile robots use regular wheels and are easy to design and build. Most mobile robot literatures are based on nonholonomic mobile robots. In this dissertation, the entire research is based on a nonholonomic differential drive WMR with two independently actuated wheels and a caster wheel.

While the WMR performance has been improved over the years for conventional applications (e.g., low speed maneuvering in a structured environment), it remains a challenge to operate a WMR at a high speed in an unstructured environment. When a WMR is operated at a high speed or on a slippery surface, wheel slip or skid will occur, both of which we call wheel slip in general. However, most of the works in the literature assume an ideal model for a WMR, with pure rolling constraint and without lateral motion at the wheels, and do not take wheel slip into account. Slip usually occurs for wheeled vehicles and is common in car driving when people try to make a sharp turn or a stop. This is because the static friction or the rolling friction is not capable of providing adequately high acceleration or deceleration. Wheel slip could be disastrous when people drive on highway while raining. However, for a race car driver it could be beneficial if slip is properly dealt with, e.g., slip can be used advantageously to gain speed during acceleration, or to increase maneuverability in cornering while maintaining a competitive speed.

In real dynamic environment, uncertain surface characteristics, dynamic obstacles, and high maneuverability requirement may all introduce slip and even instability. While it is necessary to study wheel slip effect for a WMR, wheel slip cannot be introduced without

the dynamics of the WMR and the traction forces. On one hand, as pointed out in this dissertation, when wheel slip is introduced into a nonholonomic WMR model, the WMR becomes an under-actuated system. For such a system, usually controlling all the degrees of freedom sacrifices the maneuverability, while only two degrees of freedom can be controlled if maneuverability is the main concern. Thus, studying slip is meaningful in real WMR applications because slip builds a connection between control and maneuverability. On the other hand, traction forces are generated due to wheel slips and are the direct driving forces for a WMR. Traction forces govern the dynamics of the whole WMR, so that the maneuverability of the WMR can be improved if the traction forces can be controlled properly. From experimental data, traction forces have been found to be nonlinearly dependent on wheel slips as shown in next Chapter. Traction force is approximately proportional to wheel slip when slip is within a certain amount, whereas the traction force is saturated and even starts to reduce when excessive slip occurs. Since the traction force determines the acceleration of the WMR, which represents the maneuverability of the WMR, controlling the traction force to its maximum improves the maneuverability whenever it is required, which will be investigated in this dissertation.

By extending the number of WMRs from single to multiple, more potential applications emerge. To name a few, there are formation control and pursuit-evasion problems. Formation control is a type of coordination of a group of autonomous robots where these robots are required to accomplish certain task while maintaining a desired geometric pattern. Moving in formation has the advantages of reducing the system cost,

increasing the robustness and efficiency of the system while providing redundancy, reconfiguration ability and structure flexibility for the system [1]. In a high speed formation control problem, wheel slip is inevitable and the introduction of slip may lead to instability of each robot and affect interconnection between one another. However, to the best of our knowledge, none of the work in the literature has introduced wheel slip to the problem and studied the slip effect, which will be investigated in this dissertation.

Pursuit-Evasion (P-E) problem is a family of problems in which one group of agents attempt to track down agents of another group in an environment. A typical example is a predator chases a prey animal around until the prey is captured. The problem becomes interesting and complicated because the agents evolve against one another in a continuous and open-ended way. The problem can be classified into non-game based and game based problems. The game-based problem, for two players, is a zero-sum game where the players have completely opposite interest. In a high speed game problem, wheel slip is inevitable. The introduction of slip may change the pursuit and evasion behavior and even lead to instability of the players. However, there is no work in the literature that has studied slip effect and pursuit evasion behavior for players subject to wheel slip, which will be investigated for WMR players in this dissertation.

In this thesis, the effect of wheel slip to a WMR is investigated. The applications of single WMR control, multiple WMR formation control and game-based pursuit-evasion problem are selected to study the wheel slip effect. In these applications, new control approaches are investigated for the WMR subject to wheel slip. Three types of controls, which are σ-process based discontinuous feedback control, input-output linearization

technique and sliding mode control, are developed to investigate the slip effect for such a WMR in different applications. The σ-process based discontinuous feedback control is applied to regulate the WMR to a given configuration. Input-output linearization technique is applied to linearize the WMR model and design linear control for path following and position tracking tasks. Sliding mode control is applied both to design observer to estimate the traction forces and to drive the lateral force to its maximum during turning motion. In addition, in the game-based P-E problem, based on the motion capability of a WMR subject to wheel slip, the concept of equivalent kinematic model for the pursuer is proposed to facilitate the study of the P-E behavior in the presence of slip.

The scope of this dissertation is as follows. In Chapter II, we present individual WMR model with wheel slip dynamics. We show that when both lateral and longitudinal wheel slip are introduced, the WMR model becomes an underactuated system with a second order nonholonomic constraint. In Chapter III, we propose a discontinuous feedback controller to achieve regulation control of the WMR, apply input-output linearization technique to achieve position tracking and path following control of the WMR and propose a sliding mode-based controller to achieve turning control for the WMR in various applications. In Chapter IV, we investigate slip effect in individual WMR application where we apply input-output linearization technique to the path following control task. In Chapter V, we investigate slip effect in multiple WMR formation control application where we apply input-output linearization technique to the formation control tasks. In Chapter VI, we investigate slip effect in a game-based P-E problem where we apply sliding mode technique to the WMR turning control and introduce the concept of

equivalent kinematic model to approximate the pursuer’s model such that pursuit-evasion behavior can be analyzed easily. Chapter VII summarizes the contribution and presents future work of the thesis.

CHAPTER II

DYNAMIC MODELING OF A WMR SUBJECT TO WHEEL SLIP

As nonholonomic WMRs have been increasingly applied to high speed operations in unstructured environments, wheel slip becomes an issue when ideal rolling assumption is not satisfied. In the ideal rolling constraint, the wheels of the WMR are assumed to roll without slipping. This first order nonholonomic constraint reduces the dimension of the state space and wheel torque has the direct control of the overall second order dynamics [2]. This ideal rolling constraint is violated when the WMR is either accelerating, or decelerating, or cornering at a high speed. If the slip is not considered, a given task may not be completed and a stable system may even become unstable due to the slip. Once wheel slip cannot be ignored, traction forces play a role in the overall dynamics.

There are a few recent papers that present approaches to model wheel slips in both WMR community and vehicle engineering community. In WMR community, [3] is one of the earliest works that considers slip in the WMR dynamic model. The authors considered small values of slip ratios on which traction force is linearly dependent. They then developed a slow manifold approach to design output feedback control law. In [4] anti-slip factor was introduced to represent the percentage of a wheel's angular velocity that reflects the wheel's forward speed. This same factor also represents the percentage of the wheel's driving force reflected effectively by the road friction. The road friction was considered as unmodeled dynamics. Neural network technique was applied to realize

optimal velocity tracking control. In [5] slip states are introduced into a generalized WMR kinematic model. In [6] slip is considered as a small, measurable, bounded disturbance in the WMR kinematic model, and a kinematic control law is developed to overcome the disturbance. In [7] longitudinal traction force is included in an omni-directional WMR model by externally measuring the magnitude of slip. However, the ideal WMR model is used in control design for simplicity. In [8] lateral traction force is introduced that was linearly dependent on lateral slip, and applied a steering control approach to lateral position tracking control for a bicycle model. In [9] longitudinal slip dynamics is considered in an omni-directional WMR model. However in the control law derivation, pure rolling was assumed to obtain a relationship between the driving torque and the traction force. In [10] both longitudinal and lateral traction are introduced which were approximated to be linearly dependent on longitudinal and lateral slip, respectively, for a reduced unicycle model for a four-wheel-drive WMR. In the controller design, slips and steering torque were control input to be designed first, and then by assuming that tire dynamics is significantly faster than the WMR dynamics, driving torque was designed to control the vehicle. In summary, in the above-mentioned works, either the slip has not been properly modeled to present slip effect for a nonholonomic WMR, or a nonlinear traction force model is not considered in control design so that the effect of traction forces to the WMR due to variation of slip can not be investigated. In this dissertation, we want to properly model wheel slip in the overall nonholonomic WMR dynamics, investigate the effect of the nonlinear traction forces to the WMR due to variation of slip, and exploit the slip and traction force such that the maneuverability of the WMR can be improved for

various applications.

In vehicle engineering community, usually traction forces are modeled rigorously for four-wheel vehicle systems. However, in many works they do not consider nonholonomic constraint equations in their model of the vehicle dynamics as found in [12][13][14]. This is mainly because position control is not a main concern and they focus more on engine, drive train and transmission dynamics and control than the vehicle body dynamics. However, in this dissertation, we focus more on the WMR body dynamics and control in applications where position control is a main concern.

In this dissertation, the WMR subject to wheel slip is modeled as in Fig. 2.1, where Pc is the center of mass of the WMR, P0 is the center of the wheel shaft, d is the distance from Pc to P0, b is the distance from the center of each wheel to P0. F1 and F2 are the longitudinal traction forces for *wheel*1 and *wheel*2, respectively. F3 is the lateral traction force. To take the slip effect into account, dynamic model needs to be studied instead of kinematic model. The equations for the dynamic WMR model are derived from Newton's Law shown in (2.1).

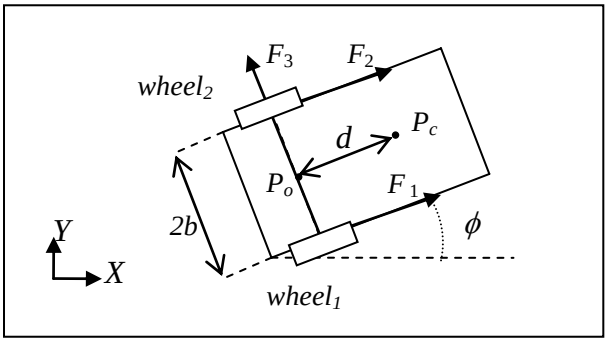

Fig. 2.1. WMR model subject to wheel slip.

$$\begin{cases} m\ddot{x}_c = (F_1 + F_2)\cos\phi - F_3\sin\phi \\ m\ddot{y}_c = (F_1 + F_2)\sin\phi + F_3\cos\phi \\ I\ddot{\phi} = (F_1 - F_2)b - F_3 d \end{cases} \tag{2.1a}$$

$$\begin{cases} I_w\ddot{\theta}_1 = \tau_1 - F_1 r \\ I_w\ddot{\theta}_2 = \tau_2 - F_2 r \end{cases} \tag{2.1b}$$

where m is the robot mass, I is its moment of inertia, Iw is the moment of inertia of each wheel about the wheel axis, r is the wheel radius, ϕ is the orientation of the WMR, θ_i is the angular displacement of the i-th wheel, τ_i is the wheel torque applied to the i-th wheel. Eq. (2.1a) represent the entire WMR dynamics in the plane motion while (2.1b) represent the spinning dynamics of the wheels.

Slip is modeled as slip angle (sr) and slip ratio (sa),

$$sr_i = \frac{r\dot{\theta}_i - v_i}{v_i}, \quad sa = \tan^{-1}(\frac{\dot{\eta}}{v}) \tag{2.2}$$

where v_i is the longitudinal speed of the center of the i-th wheel, $v = (v_1 + v_2)/2$ is the forward velocity, $\dot{\eta}$ is the lateral speed of the center of each wheel. They satisfy the following nonholonomic constraints [15]

$$\dot{v}_1 = \dot{x}_c\cos\phi + \dot{y}_c\sin\phi + b\dot{\phi} \tag{2.3}$$

$$\dot{v}_2 = \dot{x}_c\cos\phi + \dot{y}_c\sin\phi - b\dot{\phi} \tag{2.4}$$

$$\dot{\eta} = \dot{y}_c\cos\phi - \dot{x}_c\sin\phi - d\dot{\phi} \tag{2.5}$$

Note that, unlike classical nonholonomic constraints of WMR, the above constraints allow both longitudinal and lateral slips.

In order to model the slip, traction forces and design controllers, we need to have the knowledge of slip and dependency of traction forces on slip. To measure the slip, different combinations of sensors and estimation techniques have been used in the literature. In [16]

Kalman filter is adopted to estimate the slip using the data collected from wheel encoder, global positioning system (GPS) and inertial measuring unit (IMU). In [17] the amount of slip is predicted by comparing current imagery data with hitory. In [18] a purely proprioceptive navigation strategy is presented using gyro, accelerometers and wheel encoders. The states (i.e., slip accelerations) were estimated using the extended Kalman filter.

Usually the analytical dependency of traction forces on slip is difficult to formulate due to wheel temperature, thread pattern, camber angle and so on. However, the general behaviors of this dependency for rubber tire have been reported in [19]. In [20] an excellent review of current trends in modeling traction forces is provided using different methods, e.g., empirical, semi-empirical and analytical methods. Specifically, piecewise linear model, Buckhardt model, Rill model, Dahl model, Lugre model and Pacejka model or known as magic formula are discussed therein.

The Magic formula model is an elegant, semi-empirical model based on curve fitting. It has been widely accepted in industry and academia to generalize the model of both longitudinal and lateral traction forces. It was introduced in [21] and has been revised several times since then. This model has the advantage of accuracy, simplicity and ability to be interpreted over other models. Due to this reason, we employ the Magic formula model to model traction forces. In this model, the lateral and longitudinal traction forces are functions of slip angle and slip ratio as

$$F = K_1 \sin\left(K_2 \tan^{-1}\left(SK_3 + K_4\left(\tan^{-1}\left(SK_3\right) - SK_3\right)\right)\right) + S_v \tag{2.6}$$

where S is a function of slip angle for the lateral traction force or slip ratio for the

longitudinal traction force. All other variables K_i, i=1,…,4 and S_v are constants and determined from the curve fitting process of the empirical data. Fig. 2.2a shows an example of lateral traction forces with friction coefficient 0.7 and 0.3, respectively. Fig. 2.2b shows an example of longitudinal traction forces with friction coefficient 0.7 and 0.3, respectively.

Since F_i (i=1,2) is a functions of sr_i(i=1,2), sr_i(i=1,2) is a function of $\dot{\theta}_i$ (i=1,2) and $\ddot{\theta}_i$ (i=1,2) is a function of τ_i (i=1,2), $\dot{F}_i$ (i=1,2) becomes a function of τ_i (i=1,2), as shown in (2.7). Thus after taking a derivative of (2.1a), it becomes a third order system with τ_i as the input. Note that since $F1$ and $F2$ are the only control inputs to (2.1a), (2.1a) becomes an underactuated system with a second order nonholonomic constraint.

$$\dot{F}_i = \frac{K_1 K_2 \cos(K_2 \tan^{-1}(K_3 sr_i + K_4(\tan^{-1}(K_3 sr_i) - K_3 sr_i)))(K_3 + K_4(\frac{K_3}{1+K_3^2 sr_i^2} - K_3))}{1+(K_3 sr_i + K_4(\tan^{-1}(K_3 sr_i) - K_3 sr_i))^2} \frac{r v_i \tau_i - F_i r^2 v_i - r I_w \dot{\theta}_i \dot{v}_i}{I_w v_i^2} \tag{2.7}$$

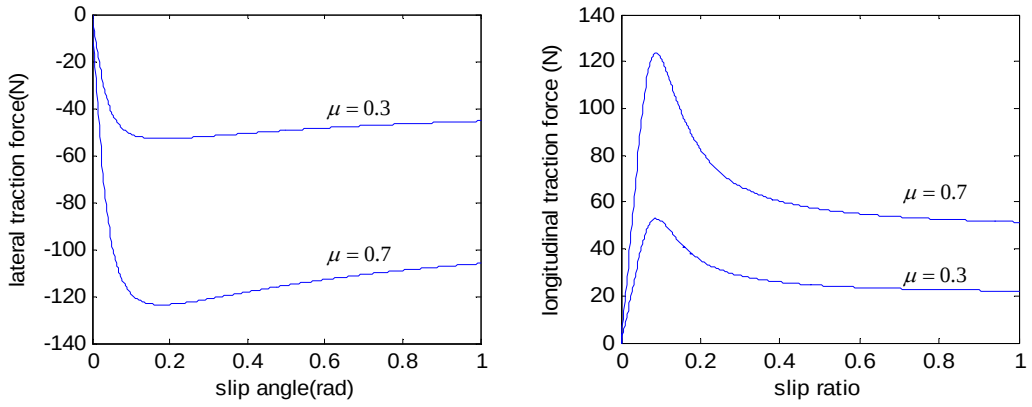

Fig. 2.2a Lateral traction for friction coefficients 0.7 and 0.3. Fig. 2.2b Longitudinal traction for friction coefficients 0.7 and 0.3.

CHAPTER III

CONTROLLER DESIGN FOR THE WMR SUBJECT TO WHEEL SLIP

In the WMR control literature, many control algorithms have been developed based on the nature of the WMR model and the applications of the WMR. Since most WMRs have nonlinear models, they are either nonlinearly controlled or linearly controlled after linearization. Backstepping control [22], Lyapunov-based control [23], sliding mode control [24], observer-based control [25] are typical nonlinear control approaches. Input-state linearization control [26], input-output linearization control [27][2][28] are typical linearized control approaches.

Once wheel slip dynamics and traction forces are introduced into the WMR model, due to the nonlinear dependence of the traction force upon wheel slip, control design becomes more difficult. Slip that is greater than a certain amount leads to traction force saturation, where slip dynamics is open-loop unstable [29][30] and may cause instability of a WMR. However, slip or traction force can be controlled such that the motion pattern of a WMR can be optimized. In vehicle control, for example, wheel slip determines the traction force upon which the maneuverability of a vehicle relies. Wheel slip can be controlled to enhance the maneuverability of a vehicle, e.g., Antilock Braking System (ABS) control. The goal of ABS control is to maintain the longitudinal traction force at its maximum during deceleration. Direct approaches drive the longitudinal traction force to its maximum using sliding mode-based extremum seeking control (ESC) [31][32][33]

without knowing the optimal slip ratio or the analytic function of the longitudinal traction force, while indirect approaches [29][30][34][35] drive the wheel slip to its optimal value, derived from estimation or sensors, where the longitudinal traction force is maximal. However, there is little research that considers the effect of lateral traction force on the motion of a WMR, which will be investigated in this chapter.

In this section, three control strategies are developed for the WMR subject to slip. They are σ-process discontinuous feedback control, sliding mode control and input-output linearization technique. In σ-process discontinuous feedback control, the WMR need to move to a desired static configuration. In sliding mode control, the WMR need to make a sharpest possible turn where the lateral traction force is maintained at its maximum. In input-output linearization technique, the WMR is controlled to achieve path following and position tracking tasks.

3.1 σ-process based Discontinuous Feedback Control

When both lateral and longitudinal slip dynamics are introduced into WMR overall dynamic model, the overall WMR model becomes a third order underactuated dynamic system with second order nonholonomic constraints. Such a model is quite different from typical ideal WMR's dynamic model in the sense that the second order nonholonomic constraint does not reduce the dimension of the state space. It has been shown that such a system is not asymptotically stabilizable to a given equilibrium solution using a time-invariant continuous feedback [38]. Therefore those control approaches for an ideal WMR dynamic model, such as backstepping technique in [36][22][37], observer based

controller in [25], cannot be applied to this model. However, such a system is asymptotically stabilizable to a desired equilibrium using time-invariant discontinuous feedback laws. In the literature, surface vessel is such a system that researchers have been working on. Surface vessel is modeled in local coordinates that is fixed on the system. It is actuated in surge and yaw direction, while non-actuated in sway direction. In [38] a discontinuous coordinate transformation named σ-process is applied to transform an underactuated surface vessel system into a discontinuous one in which the design of feedback control laws is easily carried out. Then, transforming back into the original coordinates yields discontinuous feedback laws which asymptotically stabilize the original system to the desired configuration with exponential convergence rate. In [39][40][41] the surface vessel model equations are transformed into a chained form where either discontinuous or time-varying feedback control law can be designed to asymptotically drive the system to zero. In [42] a tracking control law is developed for an underactuated surface vessel.

In this section, we transform the WMR dynamics in (2.1a) into local coordinates that is fixed on the WMR such that the non-actuated sidewise dynamics is explicit. We then apply the σ-process to transform the system into a discontinuous one, design a feedback control law and transform back to the original coordinates which yields a discontinuous controller.

3.1.1 Control law derivation

First we assume both slip ratio and slip angle are quite small and thus the traction force in (2.6) can be linearly approximated as follows [10],

$$f_{lat} = \beta \frac{\dot{\eta}}{|\dot{\rho}|}, \qquad f_{long} = \alpha \frac{\dot{\zeta}}{|\dot{\rho}|} \tag{3.1}$$

where α >0 and β <0 are constants.

For real commercial WMRs, we can only control the forward velocity *v* and the angular velocity *w* instead of wheel torques. In the pure rolling case, there is a mapping between *v*,*w* and $\dot{\theta}_1, \dot{\theta}_2$ as,

$$\begin{bmatrix} v \\ w \end{bmatrix} = \begin{bmatrix} r/2 & r/2 \\ r/2/b & -r/2/b \end{bmatrix} \begin{bmatrix} \dot{\theta}_1 \\ \dot{\theta}_2 \end{bmatrix}. \tag{3.2}$$

However, when the pure rolling is relaxed and slip is introduced, this mapping does not have physical meaning anymore. Now when we give command *v* and *w* to the WMR, we are essentially giving command $\dot{\theta}_1$ and $\dot{\theta}_2$ derived from mapping (3.2) to control the WMR dynamics (2.1a) instead of WMR kinematics. In the following steps, we consider $\dot{\theta}_1$ and $\dot{\theta}_2$ as control inputs and design feedback law to control the dynamic model as in (2.1a).

The kinematic model of the WMR is

$$\begin{bmatrix} \dot{x}_0 \\ \dot{y}_0 \\ \dot{\phi} \end{bmatrix} = \begin{bmatrix} -\sin\phi & \cos\phi & 0 \\ \cos\phi & \sin\phi & 0 \\ 0 & 0 & 1 \end{bmatrix} \begin{bmatrix} \dot{\eta} \\ v \\ w \end{bmatrix} = \begin{bmatrix} -\sin\phi & \cos\phi & 0 \\ \cos\phi & \sin\phi & 0 \\ 0 & 0 & 1 \end{bmatrix} \begin{bmatrix} 1 & 0 & 0 \\ 0 & 1/2 & 1/2 \\ 0 & 1/2/b & -1/2/b \end{bmatrix} \begin{bmatrix} \dot{\eta} \\ v_1 \\ v_2 \end{bmatrix} \tag{3.3}$$

where x_0, y_0, ϕ denote the configuration of point P_0 in Fig. 2.1, and since $x_c = x_0 + d\cos\phi, y_c = y_0 + d\sin\phi$, the dynamic model in (2.1a) can be transformed into

$$M\dot{\upsilon} + C(\dot{\phi})\upsilon = F, \tag{3.4}$$

where $\upsilon = [\dot{\eta} \quad v_1 \quad v_2]^T$, $F = [F_3 \quad F_1 \quad F_2]$, $C = \frac{m}{2}\dot{\phi}\begin{bmatrix} 0 & 1 & 1 \\ -1 & 0 & 1 \\ -1 & -1 & 0 \end{bmatrix}$,

$$M^{-1} = \begin{bmatrix} A & -bB & bB \\ -bB & E-bD & E+bD \\ bB & E+bD & E-bD \end{bmatrix}.$$ (A,B,D,E are nonzero constants [Appendix A])

When we define new state variables z_1, z_2, z_3, z_4, z_5, z_6 as

$$\begin{aligned} z_1 &= -x_0 \sin\phi + y_0 \cos\phi - \frac{bB}{D}\phi \\ z_2 &= x_0 \cos\phi + y_0 \sin\phi \\ z_3 &= \phi \\ [z_4, z_5, z_6]^T &= M\upsilon \end{aligned} \tag{3.5}$$

we will have a new set of equations as

$$\dot{z}_1 = (A + \frac{bBB}{D} + Bz_2)z_4 + Dz_2(z_5 + z_6) \tag{3.6}$$

$$\dot{z}_2 = -B(z_1 + \frac{bB}{D}z_3)z_4 + (E - Dz_1 - bBz_3)z_5 + (E + Dz_1 + bBz_3)z_6 \tag{3.7}$$

$$\dot{z}_3 = -Bz_4 - Dz_5 + Dz_6 \tag{3.8}$$

$$\dot{z}_4 = -(-Bz_4 - D(z_5 - z_6))mE(z_5 + z_6) + \beta(Az_4 - bB(z_5 - z_6))(\left|-bBz_4 + E(z_5 + z_6) - bD(z_5 - z_6)\right|^{-1} + \left|bBz_4 + E(z_5 + z_6) + bD(z_5 - z_6)\right|^{-1}) \tag{3.9}$$

$$\dot{z}_5 = u_1 \tag{3.10}$$

$$\dot{z}_6 = u_2 \tag{3.11}$$

where $u_1 = \frac{1}{2}m\dot{\phi}(\dot{\eta} - v_2) + \alpha\frac{r\dot{\theta}_1 - v_1}{v_1}$, (3.12)

$$u_2 = \frac{1}{2}m\dot{\phi}(\dot{\eta} + v_1) + \alpha\frac{r\dot{\theta}_2 - v_2}{v_2} \tag{3.13}$$

As stated in [38], such a system cannot be exponentially stabilized at an equilibrium using smooth feedback, and it is not asymptotically stabilizable to a desired equilibrium solution using time-invariant continuous feedback. Define $z=(z_1,z_2,z_3,z_4,z_5,z_6)^T \in \mathbf{M}$, and the set of equilibrium manifold $\mathbf{M}^e=\{z \in \mathbf{M} | z_4=z_5=z_6=0\}$, follow [38] and one can prove that the system described by (3.6-3.11) is strongly accessible on $\mathbf{M}$, and it is small-time locally controllable at any equilibrium $z^e \in \mathbf{M}^e$.

Now we design a time-invariant discontinuous feedback control law for the above

system. We focus only on the problem of feedback stabilization to the origin, i.e., z^e=0.

3.1.1.1 Stabilization of the reduced system

We first study the following reduced order system, which is obtained by considering the subsystem in (3.6-3.9), letting (z_5+z_6, z_5-z_6) to be the control variables (v_1,v_2):

$$\dot{z}_1 = (A + \frac{bBB}{D} + Bz_2)z_4 + Dz_2 v_2 \tag{3.14}$$

$$\dot{z}_2 = -B(z_1 + \frac{bBz_3}{D})z_4 + Ev_1 - D(z_1 + \frac{bBz_3}{D})v_2 \tag{3.15}$$

$$\dot{z}_3 = -Bz_4 - Dv_2 \tag{3.16}$$

$$\dot{z}_4 = -(-Bz_4 - Dv_2)mEv_1 + \beta(Az_4 - bBv_2)(\left|- bBz_4 + Ev_1 - bDv_2\right|^{-1} + \left|bBz_4 + Ev_1 + bDv_2\right|^{-1}) \tag{3.17}$$

Consider the above reduced system in (3.14-3.17). Restricting consideration to $z_3 \neq 0$, we apply the σ-process in [38]

$$y_1 = z_3, x_2 = z_2, x_3 = \frac{z_1}{z_3}, x_4 = \frac{z_4}{z_3} \tag{3.18}$$

to obtain

$$\dot{y}_1 = -By_1 x_4 - Dv_2 \tag{3.19}$$

$$\dot{x}_2 = Ev_1 - B(y_1 x_3 + \frac{bBy_1}{D})y_1 x_4 - D(y_1 x_3 + \frac{bBy_1}{D})v_2 \tag{3.20}$$

$$\dot{x}_3 = (A + \frac{bBB}{D} + Bx_2)x_4 + \frac{Dx_2 v_2}{y_1} + \frac{x_3}{y_1}(By_1 x_4 + Dv_2) \tag{3.21}$$

$$\begin{aligned}\dot{x}_4 &= -\frac{1}{y_1}(-By_1 x_4 - Dv_2)mEv_1 \\ &+ \frac{\beta}{y_1}(Ay_1 x_4 - bBv_2)(\left|- bBy_1 x_4 + Ev_1 - bDv_2\right|^{-1} + \left|bBy_1 x_4 + Ev_1 + bDv_2\right|^{-1}) + \frac{x_4}{y_1}(By_1 x_4 + Dv_2)\end{aligned} \tag{3.22}$$

We design the feedback law to be

$$v_1 = (-l_1 x_2 - l_2 x_3)/E \quad , \tag{3.23}$$

$$v_2 = (k_1 y_1 - By_1 x_4)/D \quad , \tag{3.24}$$

where k_1>0 and l_1, l_2 are the gains, to derive the reduced closed loop system

$$\dot{y}_1 = -k_1 y_1 \tag{3.25}$$

$$\dot{x}_2 = -l_1 x_2 - l_2 x_3 - k_1 (x_3 + \frac{bB}{D}) y_1^{\ 2} \tag{3.26}$$

$$\dot{x}_3 = (A + \frac{bBB}{D}) x_4 + k_1 x_2 + k_1 x_3 \tag{3.27}$$

$$\dot{x}_4 = -k_1 m(l_1 x_2 + l_2 x_3) + k_1 x_4 + \beta((A + \frac{bBB}{D}) x_4 - k_1 \frac{bB}{D})(|\gamma_1|^{-1} + |\gamma_2|^{-1}) \tag{3.28}$$

where $\gamma_1 = -l_1 x_2 - l_2 x_3 - k_1 b y_1$ and $\gamma_2 = -l_1 x_2 - l_2 x_3 + k_1 b y_1$.

The *x*-dynamics can be rewritten as

$$\dot{x} = (A_1 + A_2(t))x + h_1(t) \tag{3.29}$$

where $A_1 = \begin{bmatrix} -l_1, & -l_2, & 0 \\ k_1, & k_1, & A + \frac{bBB}{D} \\ -k_1 l_1 m, & -k_1 l_2 m, & k_1 + \beta(A + \frac{bBB}{D})(|\gamma_1|^{-1} + |\gamma_2|^{-1}) \end{bmatrix}$ (3.30)

$$A_2(t) = \begin{bmatrix} 0 & -k_1 x_{10}^{\ 2} e^{-2k_1 t} & 0 \\ 0 & 0 & 0 \\ 0 & 0 & 0 \end{bmatrix}, \tag{3.31}$$

$$h_1(t) = [-k_1 \frac{bB}{D} y_{10}^{\ 2} e^{-2k_1 t},\ 0,\ -k_1 \beta \frac{bB}{D}(|\gamma_1|^{-1} + |\gamma_2|^{-1})]^T. \tag{3.32}$$

It can be seen that if $0<l_1<l_2$ and $k_1 + \beta(A + \frac{bBB}{D})(|\gamma_1|^{-1} + |\gamma_2|^{-1}) < 0$, the eigenvalues of matrix A_1 can be assigned arbitrarily on the left-hand side of the phase plane. Note that $k_1 + \beta(A + \frac{bBB}{D})(|\gamma_1|^{-1} + |\gamma_2|^{-1}) < 0$ can be satisfied when set an upper bound for the WMR's forward velocity. Clearly, the y_1-dynamics is globally exponentially stable at y_1=0. Moreover, since matrix A_2(t) and h_1(t) go to zero as $t \to \infty$ (note that $(|\gamma_1|^{-1} + |\gamma_2|^{-1})$, representing the lateral traction term, will disappear when z_3 converges to zero), and

$$\int_0^\infty \|A_2(t)\| dt < \infty,\ \int_0^\infty \|h_1(t)\| dt < \infty,$$

the *x* dynamics can also be globally exponentially stable at the origin *x*=0 when matrix A_1 is a Hurwitz matrix [43].

Note that in the (z_1,z_2,z_3,z_4) coordinates the control law takes the form of

$$\mathrm{v}_1(z_1, z_2, z_3, z_4) = (-l_1 z_2 - l_2 \frac{z_1}{z_3}) / E \tag{3.33}$$

$$\mathrm{v}_2(z_1, z_2, z_3, z_4) = (k_1 z_3 - B z_4) / D \tag{3.34}$$

and the reduced closed-loop system becomes

$$\dot{z}_1 = (A + \frac{bBB}{D}) z_4 + k_1 z_2 z_3 \tag{3.35}$$

$$\dot{z}_2 = -l_1 z_2 - l_2 \frac{z_1}{z_3} - k_1 z_3 (z_1 + \frac{bB}{D} z_3) \tag{3.36}$$

$$\dot{z}_3 = -k_1 z_3 \tag{3.37}$$

$$\dot{z}_4 = k_1 z_3 m(-l_1 z_2 - l_2 \frac{z_1}{z_3}) + \beta((A + \frac{bBB}{D}) z_4 - k_1 \frac{bB}{D} z_3)(\left| -l_1 z_2 - l_2 \frac{z_1}{z_3} - k_1 b z_3 \right|^{-1} + \left| -l_1 z_2 - l_2 \frac{z_1}{z_3} + k_1 b z_3 \right|^{-1}) \tag{3.38}$$

It can be shown that both the trajectory ($z_1(t)$,$z_2(t)$,$z_3(t)$,$z_4(t)$) and (v_1(t),v_2(t)) are bounded for all $t \geq 0$ and they converge exponentially to zero. Moreover, the control law in (3.32-3.33) drives the system in (3.35-3.38) to the origin, while avoiding the set

$$N = \{(z_1, z_2, z_3, z_4) \mid z_3 = 0, (z_1, z_2, z_4) \neq 0\}.$$

3.1.1.2 Stabilization of the complete system

Now we study the problem of asymptotic stabilization of the complete system in (3.6-3.11), with u_1 and u_2, instead of x_5 and x_6, as control inputs. However, the integrator back-stepping approach developed for smooth systems cannot be directly applied here to derive control inputs due to the discontinuous nature of the system.

Consider the controllers satisfying the following equations:

$$u_1(z) + u_2(z) = -K(z_5 + z_6 - \mathrm{v}_1(z_1, z_2, z_3, z_4)) + s_1(z) \tag{3.39}$$

$$u_1(z) - u_2(z) = -L(z_5 - z_6 - \mathrm{v}_2(z_1, z_2, z_3, z_4)) + s_2(z) \tag{3.40}$$

where v_1 and v_2 are feedback laws for reduced system, and s_1 and s_2 correspond to their time derivatives along (3.6-3.11)

$$s_1(z) = \frac{1}{E}(l_1(-B(z_1 + \frac{bB}{D}z_3)z_4 + E(z_5 + z_6) - (Dz_1 + bBz_3)(z_5 - z_6))$$
$$+ \frac{l_2}{z_3}((A + \frac{bBB}{D} + Bz_2)z_4 + Dz_2(z_5 + z_6)) + l_2\frac{z_1}{z_3}(Bz_4 + D(z_5 - z_6)))$$

$$s_2(z) = \frac{1}{D}(-k_1(Bz_4 + D(z_5 - z_6)) + B(Bz_4 + D(z_5 - z_6))mE(z_5 + z_6) - B\beta(Az_4 - bB(z_5 - z_6))$$
$$(\left|-bBz_4 + E(z_5 + z_6) - bD(z_5 - z_6)\right|^{-1} + \left|bBz_4 + E(z_5 + z_6) + bD(z_5 - z_6)\right|^{-1}))$$

The idea is to implement the control law in (3.33-3.34) through the integrators by choosing gains K and L appropriately.

Consider the coordinate transformation

$$y_1 = z_3, x_2 = z_2, x_3 = \frac{z_1}{z_3}, x_4 = \frac{z_4}{z_3}, w_1 = z_5 + z_6 + (l_1 z_2 + l_2\frac{z_1}{z_3})/E, \quad w_2 = z_5 - z_6 - (k_1 z_3 - Bz_4)/D$$

Then, it can be shown that the close-loop system can be written as

$$\dot{y}_1 = -k_1 y_1 - Dw_2 \tag{3.41}$$

$$\dot{x} = (A_1 + \tilde{A}_2(t))x + h_2(t) \tag{3.42}$$

$$\dot{w}_1 = -Kw_1 \tag{3.43}$$

$$\dot{w}_2 = -Lw_2 \tag{3.44}$$

where A_1 is the matrix given by (3.30) and

$$\tilde{A}_2(t) = \begin{bmatrix} 0 & r_1(t) & 0 \\ r_2(t) & r_2(t) & 0 \\ -l_1 m r_2(t) & -l_2 m r_2(t) & r_2(t) \end{bmatrix}$$

$$r_1(t) = -(y_{10}e^{-k_1 t} + \frac{Ew_{20}}{L - k_1}e^{-Lt})(k_1 y_{10}e^{-k_1 t} + \frac{LDw_{20}}{L - k_1}e^{-Lt})$$

$$r_2(t) = D(y_{10}e^{-k_1 t} + \frac{Dw_{20}}{L - k_1}e^{-Lt})^{-1} w_{20}e^{-Lt}$$

$$h_2(t) = [-k_1\frac{bB}{D}{y_{10}}^2 e^{-2k_1 t} - bBy_{10}w_{20}e^{-(L+k_1)t} + Ew_{10}e^{-Kt},\ 0,\ mEw_{10}e^{-Kt}(k_1 + r_2(t)) - \beta\frac{bB}{D}(k_1 + r_2(t))(\frac{1}{|\gamma_1'|} + \frac{1}{|\gamma_2'|})]^T$$

where $\gamma_1' = -l_1 x_2 - l_2 x_3 - k_1 b x_1 + Ew_{10}e^{-Kt} - bDw_{20}e^{-Lt}$

and $\gamma_2' = k_1 b x_1 - l_1 x_2 - l_2 x_3 + Ew_{10}e^{-Kt} + bDw_{20}e^{-Lt}$.

The (y_1, w_1, w_2)-dynamics is globally exponentially stable at $(y_1, w_1, w_2)=(0,0,0)$. It can be

shown that if $K>k_1$ and $y_{10}w_{10} \geq 0$ (i.e. $z_{30}(z_{50}+z_{60}+l_1 z_{20}/E)+l_2 z_{10}/E \geq 0$) then $\tilde{A}_2(t)$ and $h_2(t)$ go to zero as $t \to \infty$ and

$\int_0^\infty \left\| \tilde{A}_2(t) \right\| dt < \infty$, $\int_0^\infty \left\| h_2(t) \right\| dt < \infty$.

Thus, for any initial condition (y_{10},x_0,w_{10},w_{20}) satisfying $y_{10} \neq 0$ and $y_{10}w_{10} \geq 0$, both the trajectory $(y_1(t), x(t), w_1(t), w_2(t))$ and the control $(u_1(t), u_2(t))$ are bounded for all $t \geq 0$ and converge exponentially to zero. Furthermore, the trajectory $(z_1(t), z_2(t), z_3(t), z_4(t), z_5(t), z_6(t))$ is bounded for all $t \geq 0$ and converges exponentially to zero.

3.1.2 Simulation results

We present simulation results to validate our discontinuous controller on the WMR model that include slip dynamics. For the simulation task, the WMR parameters (refer to Fig. 2.1) are as follows: b=0.24m; d=0.05m; r=0.095m; m_r=16kg; m_w=0.5kg; I_{rz}=0.537; I_{wy}=0.0023kgm^2; I_{wz}=0.0011kgm^2. We apply our proposed controller to the stabilization problem that is subject to both lateral and longitudinal slips. The traction curve slope parameters are $\alpha = 20, \beta = -12$.

We set the origin as the desired configuration and simulate the problem with the initial position of the WMR $[x_0, y_0, \phi_0] = [-2, -1, 0]$, initial forward velocity $\upsilon_0 = 0$ and initial angular velocity $\omega_0 = 0$. The control gains are: K=0.5, L=0.5, k_1=0.044, l_1=1, l_2=2.

In Fig. 3.1 we observe that the WMR trajectory converges to the origin. Fig. 3.2 is the WMR configuration, where we observe that the WMR is able to converge to the origin with monotonically decreasing ϕ. The lateral and longitudinal slip velocities are shown in Fig. 3.3 and Fig. 3.4. It can be seen that the left side wheel needs more slip to generate

more traction than the right wheel for the WMR to take a right turn. Fig. 3.5 shows the control inputs $\dot{\theta}_1$ and $\dot{\theta}_2$, respectively. We observe that both the control inputs are bounded and converge to zero asymptotically.

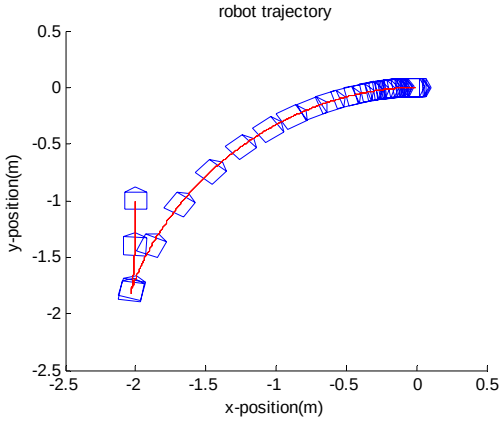

Fig. 3.1 WMR trajectory

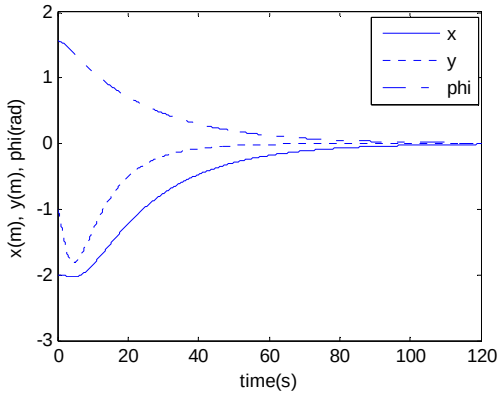

Fig. 3.2 WMR configuration

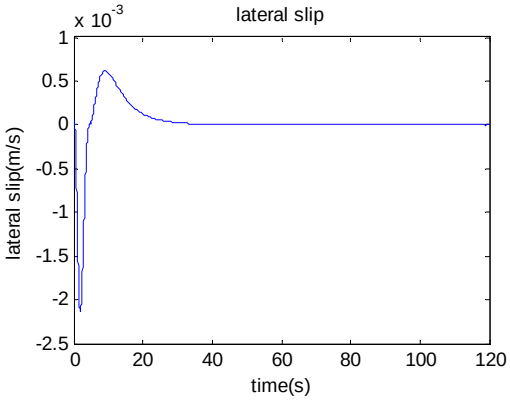

Fig. 3.3 Lateral slip velocity

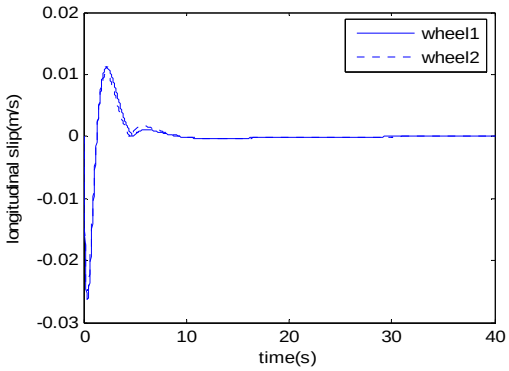

Fig. 3.4 Longitudinal slip velocity for both wheels

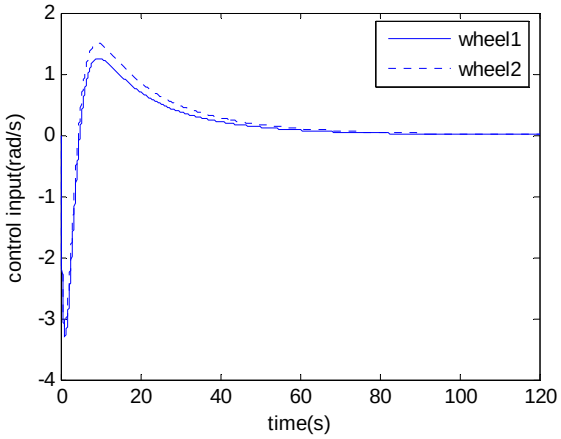

Fig. 3.5 Control inputs for wheel1 and wheel2

3.2 Sliding Mode Control

Sliding mode control is a standard approach to tackle the parametric and modeling uncertainties of a nonlinear system. It is a nonlinear control method that switches the dynamics of a nonlinear system by application of high-frequency switching control. The state-feedback control law switches from a continuous structure to another based on the current system states. Multiple control structures are designed so that the system trajectories move toward the boundaries of the control structures, i.e., sliding surface, and move along the sliding surface thereafter. Sliding mode approach transforms a higher-order system into a first-order system by designing the sliding surface, thus the control can be very simple. Lyapunov function method is applied to guarantee the stability of the nonlinear system. The main strength of sliding mode is its robustness. Since the control can be as simple as a switching between two states, it needs not be precise and will not be sensitive to parameter variations that enter the system. Additionally, since the control law is not continuous, the sliding surface can be reached in finite time.

3.2.1 Control Law Derivation

In an ABS control system of a vehicle, wheel slip has been controlled via sliding mode to maintain the longitudinal traction force at its maximum [32], such that the vehicle can stop with highest possible deceleration. In this dissertation we apply sliding mode to control a WMR to drive its lateral traction force to its maximum and maintain it during turning, such that the WMR can make a sharpest possible turn. If the optimal wheel slip is

known, where the traction force is maximal, slip can be controlled directly to maintain at its optimal value. However, when both the optimal lateral slip velocity and the analytic form of the lateral traction force are unknown, we apply a sliding mode-based extremum seeking control (ESC) approach such that the WMR conducts turning with maximum lateral traction force, which gives a minimum allowed radius of curvature for given forward velocity [44]. In addition, the longitudinal traction force is estimated via a sliding mode-based observer in [32] using the information of angular velocities of the wheels. In this dissertation, we design a sliding mode based observer to estimate the lateral traction force that will be used in the ESC design, using the information of angular velocities of both the robot and the wheels.

Since the WMR is not actuated in the lateral direction, the lateral traction force is controlled indirectly by controlling the longitudinal traction forces for the two wheels, and the longitudinal traction forces are controlled by the wheel torques. In the following section we design longitudinal traction forces both to control the lateral traction force towards its maximum and to control the forward velocity. The longitudinal traction forces are then controlled by designing input torque via standard sliding mode which is omitted in this dissertation.

3.2.1.1 Optimum Search Algorithm for Lateral Traction

Differentiating the lateral traction F_3 with respect to time along the trajectories of the system (2.11)-(2.55) we obtain

$$\frac{\mathrm{d}F_3}{\mathrm{d}t} = \frac{\partial F_3}{\partial(sa)} \frac{1}{v^2+\dot{\eta}^2} [-\frac{dbv}{I}(F_1 - F_2) - \frac{\dot{\eta}}{M}(F_1 + F_2) + F_3(\frac{v}{M} + \frac{d^2 v}{I}) - \dot{\phi}(v^2 + \dot{\eta}^2 + d\dot{\phi}\dot{\eta})] + \frac{\partial F_3}{\partial t} \tag{3.45}$$

Define an error variable $e = F_3 - F_3^r$ where F_3^r is an upper bound of F_3. Then the dynamics for *e* is governed by

$$\frac{\mathrm{d}e}{\mathrm{d}t} = \frac{\partial F_3}{\partial (sa)} \frac{v}{v^2 + \dot{\eta}^2} [A(\dot{\eta}, \dot{\phi}, v, F_1, F_2) + Bu_1] + \frac{\partial F_3}{\partial t} \tag{3.46}$$

where

$$A(\dot{\eta}, \dot{\phi}, v, F_1, F_2) = -\frac{\dot{\eta}}{Mv}(F_1 + F_2) + F_3(\frac{1}{M} + \frac{d^2}{I}) - \dot{\phi}(v^2 + \dot{\eta}^2 + d\dot{\phi}\dot{\eta})/v, \tag{3.47}$$

$$B = -\frac{db}{I}, \tag{3.48}$$

and u_1 is the new control input defined as u_1=F_1-F_2.

We design the sliding surface as

$$s = e + \int_0^t \lambda e \mathrm{d}\tau, \tag{3.49}$$

where $\lambda > 0$. If *s* converges to a constant, the sliding motion satisfies

$$\frac{\mathrm{d}e}{\mathrm{d}t} + \lambda e \to 0, \tag{3.50}$$

and the lateral traction force can be made to its maximum with a proper selection of λ. To obtain the control law to let *s* converge to a constant, first we rewrite (3.49) together with (3.46) as

$$\frac{\mathrm{d}s}{\mathrm{d}t} = \frac{\partial F_3}{\partial (sa)} \frac{v}{v^2 + \dot{\eta}^2} [A(\dot{\eta}, \dot{\phi}, v, F_1, F_2) + Bu_1] + \frac{\partial F_3}{\partial t} + \lambda e. \tag{3.51}$$

Let $A = \overline{A} + \Delta A$ where $\overline{A}$ represent the nominal part of *A* whereas the unknown part ΔA is bounded by $|\Delta A| \le \delta A$. Design the control law as

$$u_1 = -B^{-1}(\overline{A} + \gamma \Phi(s)), \tag{3.52}$$

where $\gamma = \delta A + N$ with *N*>0,

and $\Phi(s) = \mathrm{sgn}\sin(2\pi s/\alpha)$, a periodic switching function [31][32], which periodically search the traction force neighborhood to determine the control direction. This selection

guarantees that s converges to $k\alpha$ for some integer k, which depends on the initial condition and F_3^r, if the following sliding mode existence condition is satisfied:

$$\left|\frac{\partial F_3}{\partial(sa)}\frac{v}{v^2+\dot{\eta}^2}(\delta A+N)\right|>\left|\frac{\partial F_3}{\partial(sa)}\frac{v}{v^2+\dot{\eta}^2}\Delta A+\frac{\partial F_3}{\partial t}+\lambda e\right|. \tag{3.53}$$

If it is assumed that the explicit dependence of traction on time is negligible, and keep in mind that $|\Delta A|\le\delta A$, the sliding mode existence condition turns into

$$\left|\frac{\partial F_3}{\partial(sa)}\right|\frac{v}{v^2+\dot{\eta}^2}N>\lambda|e|. \tag{3.54}$$

Thus in sliding mode, the lateral traction force will converge to F_3^r until it enters a region where the gradient is so small that the condition (3.53) cannot be satisfied. When (3.53) is not satisfied, the traction is close to its maximum and it will behaves arbitrarily. However, for a given F_3^r and λ, we can select a sufficiently large N such that this region around the maximum can be made arbitrarily small. In future simulations we select λ=0.5 and α=0.5.

3.2.1.2 Forward Velocity Control

From (2.1-2.5) we obtain that the forward velocity is governed by

$$M\dot{v}=F_1+F_2+M\dot{\phi}(\dot{\eta}+d\dot{\phi}), \tag{3.55}$$

which we rewrite as

$$M\dot{v}=u_2+M\dot{\phi}(\dot{\eta}+d\dot{\phi}), \tag{3.56}$$

where u_2 is the new control input defined as $u_2=F_1+F_2$.

We design sliding surface as

$$s=v-v_r \quad , \tag{3.57}$$

where v_r is the desired speed. If s converges to zero, v will converge to v_r. The sliding

surface is governed by

$$\dot{s} = \frac{u_2}{M} + \dot{\phi}(\dot{\eta} + d\dot{\phi}) = \frac{u_2}{M} + C(\dot{\phi}, \dot{\eta}) . \tag{3.58}$$

Let $C = \overline{C} + \Delta C$ where $\overline{C}$ represents the nominal part of C whereas the unknown part ΔC is bounded by $|\Delta C| \le \delta C$.

Design the control law as

$$u_2 = -M\overline{C} + Mk\,\mathrm{sgn}(s) , \tag{3.59}$$

where $k = \delta C + \mu$ with $\mu > 0$, such that s converges to zero.

3.2.1.3 Lateral Traction Observer

The realization of the ESC algorithm requires the knowledge of the lateral traction force. We assume this quantity cannot be measured directly, so we develop an observer which allows us to obtain lateral traction force using the measurements of the robot angular velocity $\dot{\phi}$ and the wheel angular velocity $\dot{\theta}_i$. This observer is based on the equivalent control method, which has been used to develop observer for longitudinal traction force in ABS control in [32].

From (2.1) we obtain the dynamic equation

$$Ir\ddot{\phi} + I_w b(\ddot{\theta}_1 - \ddot{\theta}_2) = (\tau_1 - \tau_2)b - F_3 rd . \tag{3.60}$$

Now we define a new variable $\zeta = \dot{\phi} + \frac{I_w b}{Ir}(\dot{\theta}_1 - \dot{\theta}_2)$, which turns (3.60) into

$$Ir\dot{\zeta} = (\tau_1 - \tau_2)b - F_3 rd . \tag{3.61}$$

We define an estimate $\hat{\zeta}$ which satisfies

$$Ir\dot{\hat{\zeta}} = (\tau_1 - \tau_2)b - Vrd \quad . \tag{3.62}$$

The function V is picked as

$$V = -N\,\mathrm{sgn}(\overline{\zeta}) \tag{3.63}$$

where $\bar{\zeta} = \zeta - \hat{\zeta}$ is a tracking error of ζ and N>0 is a sufficiently large constant.

Subtracting (3.62) from (3.61) we obtain

$$Ir\dot{\bar{\zeta}} = -rdN\,\mathrm{sgn}(\bar{\zeta}) - rdF_3 . \tag{3.64}$$

If N is selected such that $N > \max\{|F_3|\}$, $\bar{\zeta}$ converges to the sliding surface $\bar{\zeta} = 0$. On sliding surface the equivalent value of variable $V = -N\,\mathrm{sgn}(\bar{\zeta})$ is equal to F_3

$$V_{eq} = F_3 \quad . \tag{3.65}$$

As shown in [32], the equivalent value of the high frequency switching signal can be obtained by applying a low pass filter

$$H(s) = \frac{1}{T_f s + 1} \quad , \tag{3.66}$$

where T_f is the constant which suppresses the high frequency signal. Since this chattering only occurs in the lateral traction force observer loop, it will not affect the entire system. The estimate of the lateral traction force out of the filter will be used in the ESC algorithm.

3.2.1.4 Longitudinal Traction Force Tracking

From previous sections *A* and *B*, we obtain desired F_1 and F_2 to control lateral traction force and forward velocity. Now, we design τ_i to enable F_i to track desired F_i using sliding mode control, which is omitted in this dissertation.

3.2.2 Simulation Results

Refer to section 4.2 for simulation results.

3.3 Input-Output Linearization Technique

3.3.1 Path Following Control

In Chapter II, wheel slip dynamics was modeled in a WMR's overall dynamics. Although such a system with nonholonomic constraints is not input-state linearizable, it may be input-output linearizable if proper outputs are chosen [2]. In this section, we choose two outputs h_1 and h_2 for the look-ahead point P_l on the WMR. h_1 is defined as the shortest distance from the look-ahead point to the desired path. h_2 is defined as forward velocity of the WMR, which is the velocity component of the look-ahead point along the *x*-axis on the WMR local frame. The input-output linearization was also applied to approach path following control for the WMR in [15].

3.3.1.1 Control law derivation

Based on the dynamic model presented in Chapter II, we approach the path following control problem of a WMR. Referring to Fig. 2.1, the coordinates of the look-ahead point P_l are given by,

$$x_l = x_c + l\cos\phi$$

$$y_l = y_c + l\sin\phi \tag{3.67}$$

Let the output equation be represented by a vector *y*, where,

$$y = h = \left[h_1(q) \quad h_2(\dot{q})\right] \tag{3.68}$$

where $q = [x_c, y_c, \phi]^T$ and $\upsilon = [\dot{\eta}, v_1, v_2]^T$.

Since any set of paths can be constructed through a combination of circular and straight-line segments [45], we develop explicit equations for $h_1(q)$ for both circular and

straight-line paths. For a circular path $h_1(q)$ can be formulated as follows,

$$h_1(q) = \sqrt{\left((x_l - x_f)^2 + (y_l - y_f)^2\right)} - R \tag{3.69}$$

$P_f = (x_f, y_f)$ is the instant center of circular path with respect to an inertial frame and R is the instantaneous radius of the circular path. Points $P_l = (x_l, y_l)$ (the look-ahead point) and $P_c = (x_c, y_c)$ (the center of mass) are related through (3.69).

As for a straight-line path, the output equation becomes,

$$h_1(q) = \frac{C_1 x_l + C_2 y_l + C_3}{\sqrt{C_1^{\,2} + C_2^{\,2}}} \tag{3.70}$$

where all $C_i, i = 1,2,3$ are constants used to describe the straight-line. From (3.69-3.70), we see the shortest distance between the look-ahead point and the path can be taken as the absolute value of h_1. After the introduction of longitudinal slip, the forward velocity of the WMR can be written as follows,

$$h_2(\dot{q}) = \dot{x}_c \cos\phi + \dot{y}_c \sin\phi \quad . \tag{3.71}$$

Now, we proceed to develop a nonlinear controller based on the feedback linearization technique. The decoupling matrix for feedback linearization for the above output equations are differentiated until the input terms appear in the output equations such that,

$$\dot{y}_1 = \frac{\partial h_1}{\partial q}\dot{q} = J_{h_1}\dot{q}, \quad \ddot{y}_1 = \frac{\partial J_{h_1}}{\partial q}\dot{q}^2 + J_{h_1}\ddot{q}, \quad \dddot{y}_1 = \frac{\partial^2 J_{h_1}}{\partial q^2}\dot{q}^3 + 3\frac{\partial J_{h_1}}{\partial q}\dot{q}\ddot{q} + J_{h_1}\dddot{q} \tag{3.72}$$

$$\dot{y}_2 = \frac{\partial h_2}{\partial \dot{q}}\ddot{q} = J_{h_2}\ddot{q}, \quad \ddot{y}_2 = \frac{\partial J_{h_2}}{\partial \dot{q}}\ddot{q}^2 + J_{h_2}\dddot{q}.$$

As an example, for the straight-line path,

$$J_{h_1} = \frac{1}{\sqrt{C_1^{\,2} + C_2^{\,2}}}\begin{bmatrix} C_1 & C_2 & C_2 l\cos\phi - C_1 l\sin\phi & 0 & 0 & 0 & 0 \end{bmatrix} \quad \text{and} \quad J_{h_2} = \begin{bmatrix} \cos\phi & \sin\phi & 0 \end{bmatrix} \quad .$$

$J_{h_i} = \frac{\partial h_i}{\partial q}$ is known as the *Jacobian* matrix and we can use them to compute the

decoupling matrix, Φ as follows,

$$\Phi = \begin{bmatrix} J_{h_1} \\ J_{h_2} \end{bmatrix} \tag{3.73}$$

We utilize the decoupling matrix to establish the input-output feedback linearization as shown below,

$$\ddot{y} = \begin{bmatrix} \ddot{y}_1 \\ \ddot{y}_2 \end{bmatrix} = \begin{bmatrix} \ddot{J}_{h_1} \\ 0 \end{bmatrix} \dot{q} + \left(\begin{bmatrix} \dot{J}_{h_1} \\ 0 \end{bmatrix} + \dot{\Phi} \right) \ddot{q} + \Phi \dddot{q} \tag{3.74}$$

If we represent (3.74) in the form of $\ddot{y} = U + V\dddot{q}$, where $\dddot{q}$ is a function of $\dot{F}$ as in (2.1) and $\dot{F}$ is a function of wheel torque as in (2.7), we can have dynamics between input and output as $\ddot{y} = P + Q\tau$. If we design a new control input to be $u_d = P + Q\tau$, the system is linearized to be $\ddot{y} = u_d$, for which we can design a linear controller as,

$$u_d = \ddot{y}_{desired} + K_i \ddot{e} + K_v \dot{e} + K_p e \tag{3.75}$$

where $e = h_{i\_desired} - h_{i\_actual}$ and K_i, K_v and K_p are control gains for the linear system.

Then the torque input to the original nonlinear system becomes

$$\tau = Q^{-1}(u_d - P) \tag{3.76}$$

3.3.1.2 Simulation results

Refer to *Case III* in section 4 for simulation results.

3.3.2 Position Tracking Control

3.3.2.1 Control Law Derivation

We choose x and y coordinates of the look-ahead point P_l in Fig. 2.1 as the outputs to be controlled, which is $y = h(q) = \begin{bmatrix} x_l \\ y_l \end{bmatrix} = \begin{bmatrix} x_c + l\cos\phi \\ y_c + l\sin\phi \end{bmatrix}$. Then following the steps in Section 3.3.1, the system will be feedback linearized and linear control law will be derived in the form of (3.76).

3.3.2.2 Simulation Results

Straight Line Tracking. Figure 3.6 shows the WMR tracking a desired trajectory {(x,y)|x=1,y=3t} with the WMR's center starting from $[x_0, y_0, \phi_0] = [-2,0,0]$ (the dotted line is the path of the look-ahead point). The control gains are $k_{p1}=k_{p2}=$ 1600, $k_{v1}=1600$, $k_{v2}=1600$, $k_{i1}=3$, $k_{i2}=3$, initial speed is 3m/s, same as the desired speed, and the ground friction coefficient is 0.3. We observe in Fig. 3.7 that the position tracking error converges to zero. In Fig. 3.8 we observe that the WMR's lateral slip converges to zero at its steady state. The maximal lateral slip is about 1.5m/s, and the corresponding slip angle can be calculated from (2.2) to be about 26 degree, meaning that the lateral force is in saturation at that time. This shows that even though the lateral force is saturated, the system is still able to accomplish the tracking task. Obviously in the cases where the lateral force is never saturated (either low desired velocity or high surface friction coefficient), the tracking task can be accomplished as well.

Circular Tracking. Figure 3.9 shows the WMR tracking a desired trajectory {(x,y)|x=5cos(0.2t), y=5sin(0.2t)} with the WMR's center of mass starting from $[x_0, y_0, \phi_0] = [0,0,0]$. The control gains are $k_{p1}=k_{p2}=16e+4$, $k_{v1}=16e+4$, $k_{v2}=16e+4$, $k_{i1}=3$, $k_{i2}=3$, initial speed is 1m/s, same as the desired speed, and the friction coefficient is 0.3. We observe in Fig. 3.10 that the tracking error converges to zero. In Fig. 3.11 we observe that the lateral slip converges to a value whose corresponding lateral force is not saturated.

In Fig. 3.12, the WMR tracks a trajectory {(x,y)|x=5cos(t), y=5sin(t)} with the WMR's center starting from $[x_0, y_0, \phi_0] = [5,0,\pi/2]$. The initial speed is 5m/s, same as the

desired speed. The control gains are same as above. We observe in Fig. 3.12 that the WMR does not have a good tracking. From Fig. 3.13 we see that the lateral slip is in the region where the lateral force is always in saturation. The lack of traction force explains the bad tracking behavior.

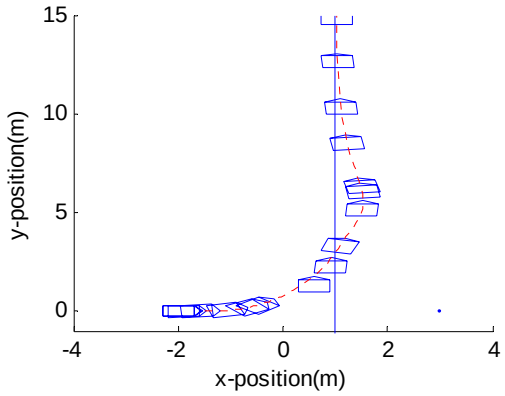

Figure 3.6. Straight line tracking

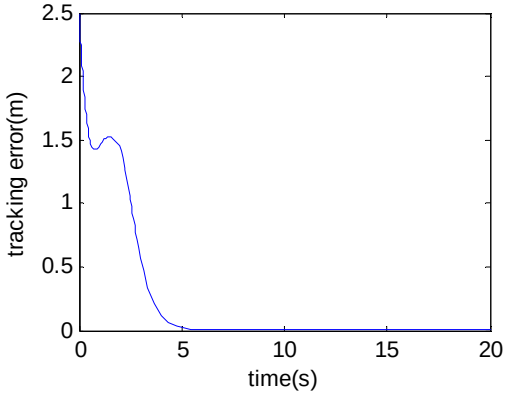

Figure 3.7. Position tracking error

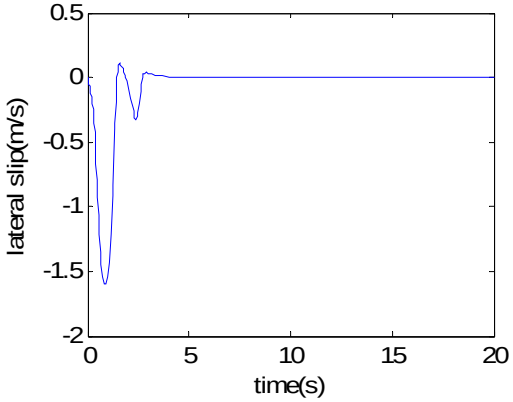

Figure 3.8. Lateral slip

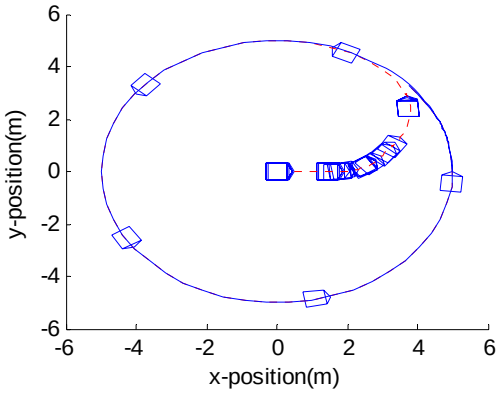

Figure 3.9. Circular tracking

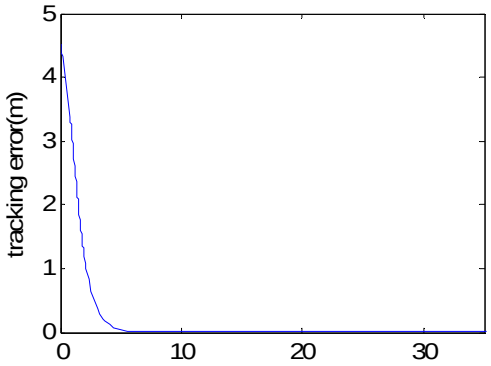

Figure 3.10. Tracking error

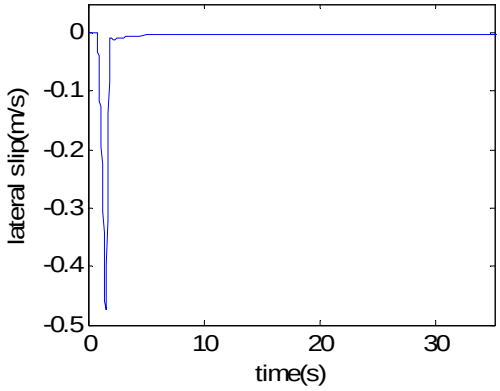

Figure 3.11. Lateral slip

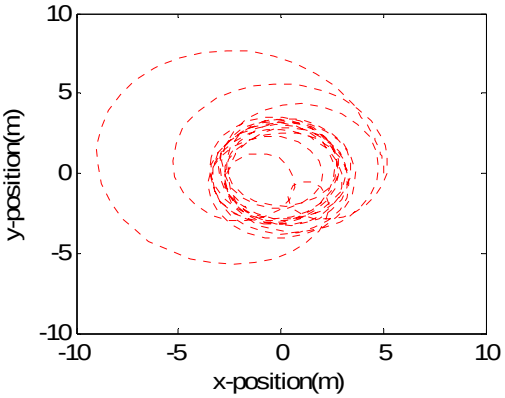

Figure 3.12. Circular tracking

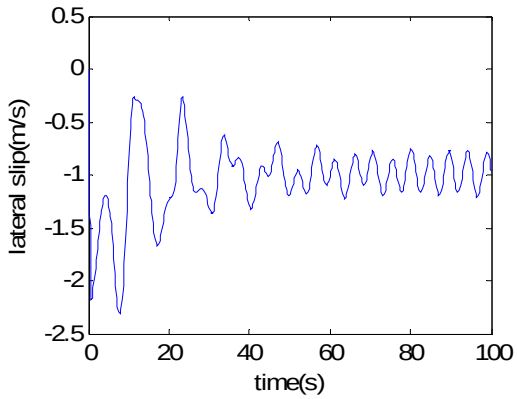

Figure 3.13. Lateral slip

CHAPTER IV

APPLICATION I: SINGLE ROBOT CONTROL

4.1 Single Robot Path Following Control

In this section, we investigate how wheel slip affects the performance of individual WMR. We focus on three different path following control cases and compare the effect of slip. From now on, we call the WMR model with slip information the slipping model, and WMR model without the slip information the no-slipping model. And we call the WMR controller with slip information the slipping controller, and the WMR controller without slip information no-slipping controller. *Case I* is for WMR with no-slipping model and no-slipping controller. *Case II* is for WMR with slipping model and no-slipping controller. *Case III* is for WMR with slipping model and slipping controller. In these three cases, all the WMR models are input-output linearizable. Therefore the path following control can be applied to them. To focus on comparing slip effect in these cases, it is better to let all other information be as much same as possible. First, they have the same path and desired speed to follow. Second, their linearized close-loop models are the same in the frequency domain. Last, we let their initial condition and the surface friction coefficient to be the same.

Case I: No-slipping model with no-slipping controller

In this case, the WMR, with no-slipping model and no-slipping controller, starts at point $[x_0, y_0, \phi_0] = [0,0,0]$ and follows an *L*-shape path with an initial speed of 2.5m/s,

which is also the desired speed. The *L*-shape path consists of straight line L_1={(x,y)|y=0,x<10} and L_2={(x,y)|x=10,y>=0}. In the linearized close-loop model, the transfer functions for distance and velocity inputs are

$$H_{dis}(s) = \frac{k_p}{s^2 + k_{v1}s + k_p}, \qquad H_{vel}(s) = \frac{k_{v2}}{s + k_{v2}} \tag{4.1}$$

and we choose the control gains k_p=9, k_{v1}=3, k_{v2}=1. Since there is no wheel slip, the WMR is able to take a sharp turn in a stable manner, which can be observed in Fig. 4.1.

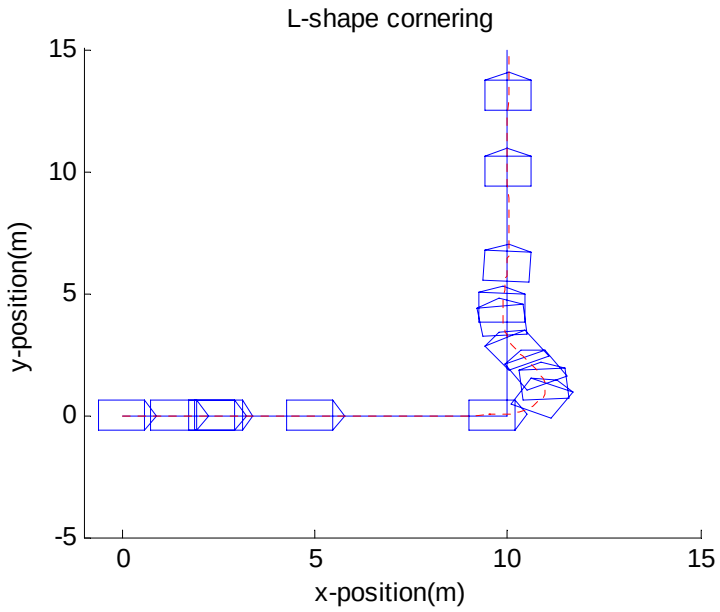

Fig. 4.1 *L*-shape cornering for single WMR with no-slipping model and no-slipping controller

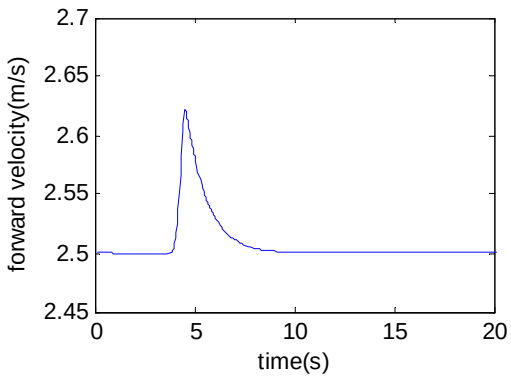

Fig. 4.2 Forward velocity

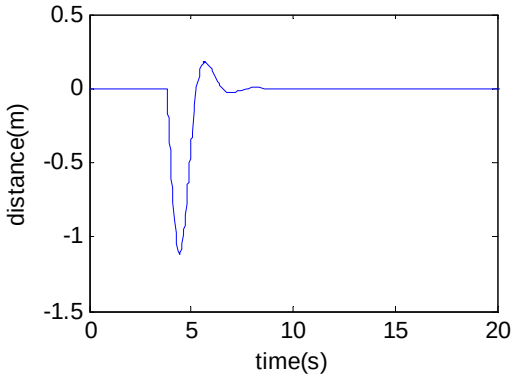

Fig. 4.3 Distance from the desired path

From Fig. 4.2 and Fig. 4.3 we observe that, starting from the corner point, it takes the WMR only about 5 seconds to converge to the stable state.

Case II: Slipping model with no-slipping controller

In this case, the WMR with slipping model and no-slipping controller follows the same *L*-shape path as in *Case I* with the same initial speed and desired speed of 2.5m/s. The control gains are k_p=9, k_{v1}=3, k_{v2}=1, which are same as those in *Case I*. The surface friction coefficient is 0.3, which represents a slippery surface. Since the controller does not know the slip and it controls the WMR as if there is no slip, the WMR is subject to unstable behavior, which can be observed in Fig. 4.4.

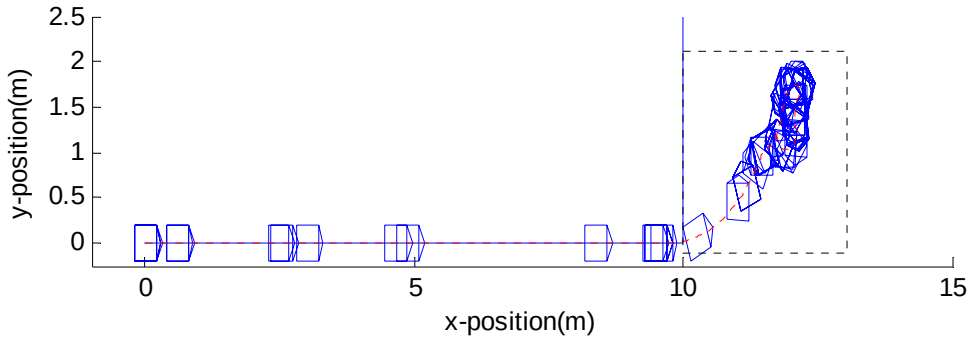

Fig. 4.4 *L*-shape cornering for single WMR with slipping model and no-slipping controller

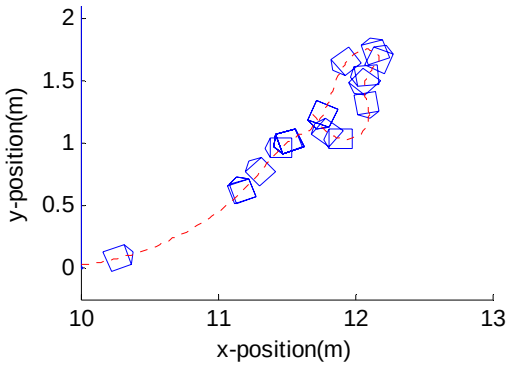

Fig. 4.5 Dotted area in Fig. 4.4

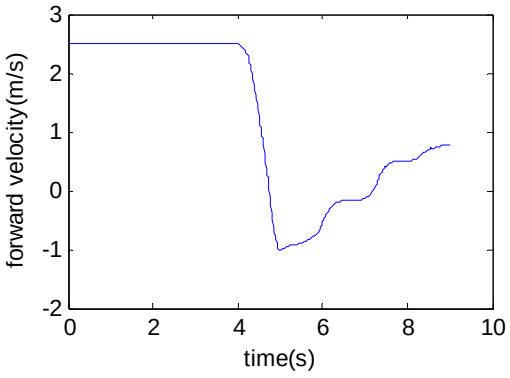

Fig. 4.6 Forward velocity

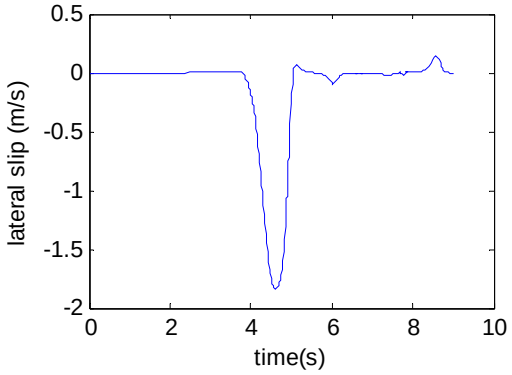

Fig. 4.7 Lateral slip velocity

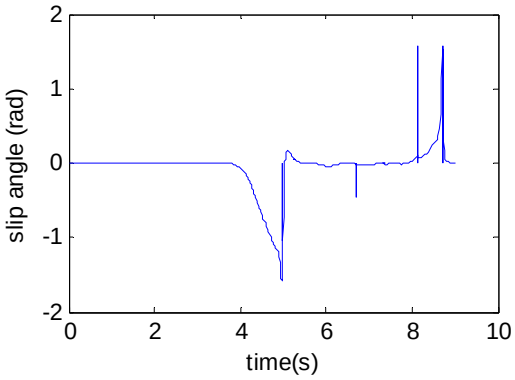

Fig. 4.8 Slip angle

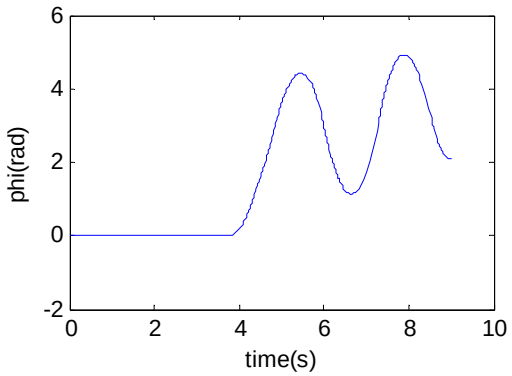

Fig. 4.9 Robot orientation

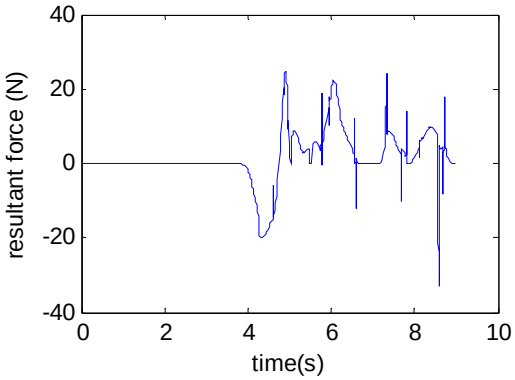

Fig. 4.10 Resultant tangential force along heading direction

We observe in Fig. 4.4 and Fig. 4.5 that the WMR falls into instability after it starts cornering. From Fig. 4.6 we observe that the WMR's forward speed is reduced to below zero, meaning that the WMR is moving backward at that moment, which we will explain shortly. In Fig. 4.7-4.8, we observe that the lateral slip is so much that the slip angle enters the region where lateral traction is reducing as slip angle increases (see Fig. 2.2). In Fig. 4.9, the orientation shows that the WMR swings back and forth in an unstable manner. Fig. 4.10 shows the component of the resultant tangential force along heading direction of the WMR, which is derived as follows.

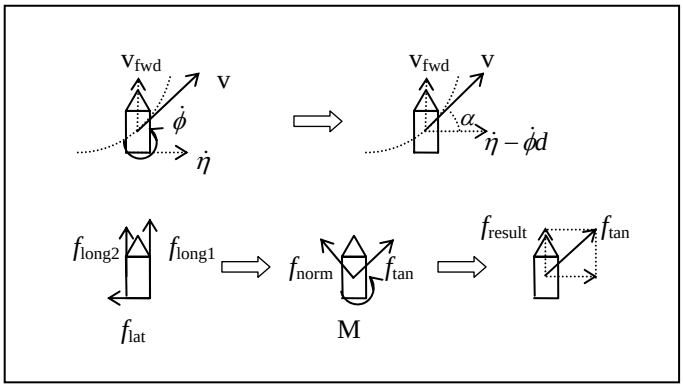

Fig. 4.11 Derivation of resultant force in Fig. 4.10

In Fig. 4.11, the dotted curve is the WMR's path, α is the angle between actual velocity and positive *x*-axis. f_{long1}, f_{long2} and f_{lat} are obtained from the simulation results. f_{norm} is the resultant normal force, f_{tan} is the resultant tangential force and M is the resultant torque. The component of the tangential resultant force along the heading direction is calculated as

$$f_{result} = ((f_{long1} + f_{long2})\sin\alpha - f_{lat}\cos\alpha)\sin\alpha \,. \tag{4.2}$$

This resultant force is consistent with the velocity profile in Fig. 25 in such a way that when the force is negative the velocity is decreasing, and when the force is positive the velocity is increasing. If we compare this resultant force with the corresponding force in *Case I*, the velocity decrease can be properly explained. In *Case I*, the lateral traction force does not contribute to f_{result}, and f_{result} equals to the driving force, meaning that the driving force is entirely employed to drive the WMR forward. However in *Case II*, the lateral traction force contributes a negative term to f_{result}. Because the controller does not know this contribution, it does not generate enough driving force either to drive the WMR or to balance the lateral traction effect. As a result, the actual force to drive the WMR becomes less than required and even negative along with decreasing velocity. Afterwards,

as the lateral slip starts to reduce, lateral traction force becomes smaller and longitudinal traction force dominates in the resultant force. Then the WMR is able to gain its speed again.

Case III: Slipping model with slipping controller

In this case, the WMR with slipping model and slipping controller follows the same *L*-shape path as in *Case I* with the same initial and desired speed of 2.5m/s. The surface friction coefficient is 0.3, which is a slippery surface. The control gains in the linearized close-loop model are K_p=450, K_{v1}=159, K_{v2}=50, K_{i1}=53, K_{i2}=51. These control gains are derived by letting the frequency response of the close-loop model in *Case III* be the same with that in *Case I*. The transfer functions for distance and velocity inputs in the close-loop model in *Case III* are

$$\begin{aligned} H_{dis}(s) &= \frac{K_p}{s^3 + K_{i1}s^2 + K_{v1}s + K_p} \\ H_{vel}(s) &= \frac{K_{v2}}{s^2 + K_{i2}s + K_{v2}} \end{aligned} . \tag{4.3}$$

To let (4.1) and (4.3) have same frequency response, we need to find a number a>>1 such that

$$\begin{aligned} (s+a)(s^2 + k_{v1}s + k_p) &= s^3 + K_{i1}s^2 + K_{v1}s + K_p \\ (s+a)(s + k_{v2}) &= s^2 + K_{i2}s + K_{v2} \end{aligned} . \tag{4.4}$$

We set a=50, hence K_p=a*k_p=450, K_{v1}=a*k_{v1}+k_p=159, K_{v2}=a*k_{v2}=50, K_{i1}=a+k_{v1}=53, K_{i2}=50+k_{v2}=51.

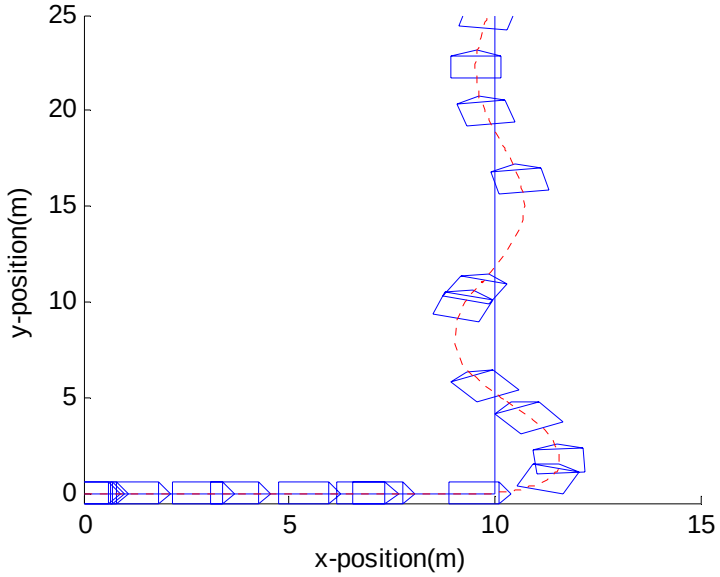

Fig. 4.12 *L*-shape cornering for a single WMR with slipping model and slipping controller

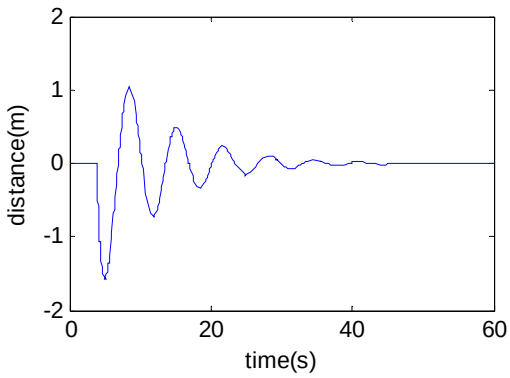

Fig. 4.13 Distance from desired path

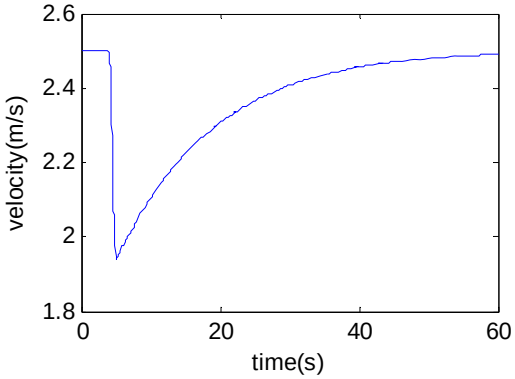

Fig. 4.14 Forward velocity

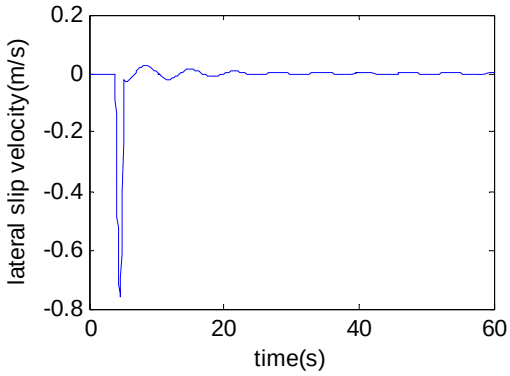

Fig. 4.15 Lateral slip velocity

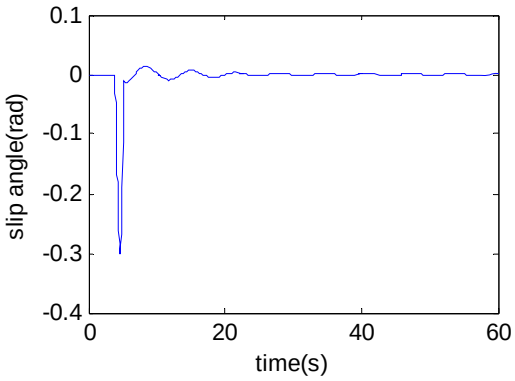

Fig. 4.16 Slip angle

From Fig. 4.12-4.14 we observe that the WMR's outputs converge to desired outputs, however, it takes longer time to converge than in *Case I*. Fig. 4.15-4.16 show lateral slip

velocity and slip angle, respectively. Compared to *Case II*, the forward velocity is not reduced by too much, and this can be explained as, since the controller knows that the lateral traction force plays a role in f_{result}, it generates more driving force to balance the effect of lateral traction and stops the velocity from reducing too much. This increase in the driving force also increases the resultant normal force. Eventually, the lateral slip is much less than that in *Case II*, which keeps the WMR in stable motion. This simulation proves the effectiveness of the controller for the WMR model with slip.

4.2 Single Robot Sharp Turning Control

Applying the sliding mode technique in Chapter III, we show turning control simulation results in this section. Let the WMR start from the configuration [0,0,0] with initial and desired velocity 2m/s. The friction coefficient is 0.3. The sliding mode control law controls the robot to make a turn at almost constant curvature in Fig. 4.17. Fig. 4.18 shows the lateral slip velocity which stays close to optimal slip value where maximum traction force occurs. In Fig. 4.19 we observe that the actual lateral traction force oscillate closely to the maximum value indicated in Fig. 6a. The estimated lateral traction force from the observer tracks the actual force nicely. Fig. 4.20 shows the wheel torque that generates switching control input for the WMR.

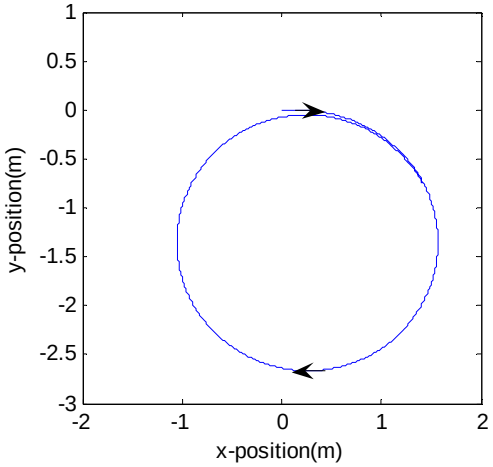

Fig. 4.17 Turning control trajectory

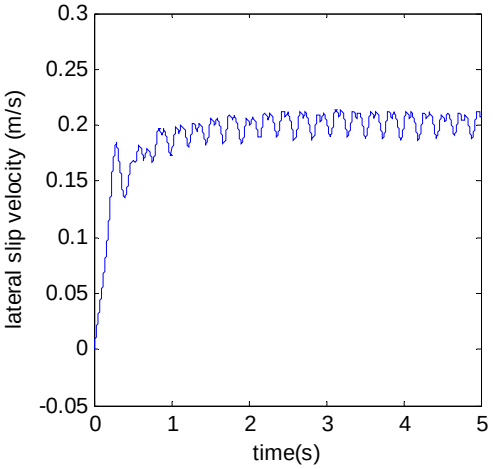

Fig. 4.18 Lateral slip velocity in turning control

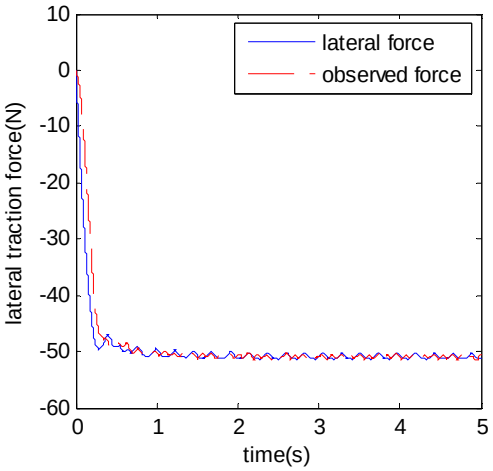

Fig. 4.19 Actual and observed lateral traction force

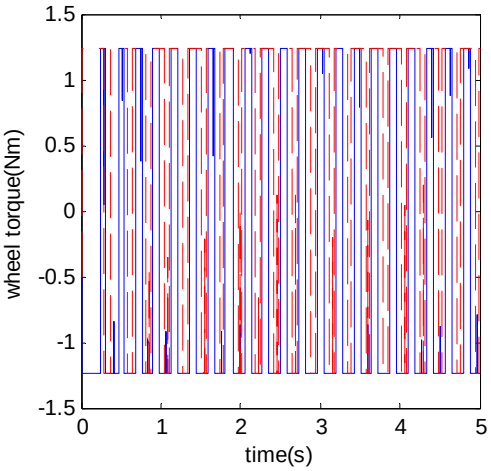

Fig. 4.20 Wheel torques

CHAPTER V

APPLICATION II: MULTI-ROBOT FORMATION COTNROL

In this section, we focus on investigating the effect of wheel slip for multiple WMRs formation. We take leader-follower formation control as a specific example, where there are three WMRs, the leader is governed by path following control and the other two followers are governed by $l-\psi$ control [46]. Briefly, the $l-\psi$ control is for a follower WMR to preserve desired inter-distance l and relative angle ψ to its leader. In [46] $l-\psi$ control was applied to follower WMRs kinematic model. In [47] velocity control inputs were derived for follower WMR having kinematic model subject to $l-\psi$ control, and backstepping technique was applied to derive torque control input for the follower's dynamic model. In [48] $l-\psi$ control was applied to follower WMR kinematics to derive velocity control input, and in order to track this velocity Lyapunov based approach was applied to derive torque control input for WMR dynamics. Since our WMR system with slip dynamics is an underactuated system as mentioned in last section, backstepping technique is not applicable. We apply input-output linearization to derive the $l-\psi$ control law for follower WMRs when outputs l and ψ are chosen.

We investigate how the WMR formation evolves during the leader's path following task, and how the formation changes subject to slip effect. We focus on three cases of formation control and compare slip effect between them. In *Case I* each WMR in the formation has no-slipping model and no-slipping controller. In *Case II* each WMR has

slipping model and no-slipping controller. In *Case III* each WMR has slipping model and slipping controller. To focus on comparing slip effect in these cases, it is better to let all other information be as much same as possible. First, in these three cases the leader WMRs have the same path to follow and the desired inter-distance and relative angle for corresponding follower WMRs are the same. Secondly, the linearized close-loop models of the WMRs are same with each other in the frequency domain. Lastly, we let their initial condition, desired velocity, surface friction coefficient to be the same.

Case I: Formation with WMRs having no-slipping model and no-slipping controller

In this case, the leader WMR starts at point $[x_0, y_0, \phi_0]=[0,0,0]$ and follows an *L*-shape path with an initial speed of 2.5m/s, which is also the desired speed. The *L*-shape path consists of straight line L_1={(x,y)|y=0,x<10} and L_2={(x,y)|x=10,y>=0}, which is same as that in Chapter III. The other two follower WMRs start from [-4,4,0], [-4,-4,0] and follow the leader while preserving desired inter-distance 5m and relative angle $\pi/4$, $3\pi/4$ to the leader. The controller for leader is same as that in *Case I* in Chapter III. The controller for the follower WMRs are $l-\psi$ controller. It depends on the states of the follower WMR and its leader. It is easy to show that, when we take second order derivative of the outputs *l* and ψ, the torque input appears. Then the transfer functions for desired *l* and ψ in the linearized close-loop model are

$$H_{dis}(s)=\frac{k_{p_d}}{s^2+k_{v_d}s+k_{p_d}},\qquad H_{ang}(s)=\frac{k_{p_a}}{s^2+k_{v_a}s+k_{pa}} \tag{5.1}$$

and we choose the control gains k_{pd}=0.5, k_{vd}=2 and k_{pa}=0.5, k_{va}=2, respectively.

In Fig. 5.1 we observe the trajectories of three WMRs follow an *L*-shape path while preserving a triangular formation. In Fig. 5.2 it shows the shape distortion along the way. Shape distortion is quantitatively determined as follows.

Definition 5.1[49] The **configuration** is the set of landmarks on a particular object. The **configuration matrix** X is the $k \times m$ matrix of Cartesian coordinates of the k landmarks in m dimensions.

Definition 5.2 An $m \times m$ rotation matrix satisfies $\Gamma^T \Gamma = \Gamma \Gamma^T = I_m$ and $|\Gamma| = 1$. The set of all m×m rotation matrices is known as the Special Orthogonal group SO(m).

Definition 5.3 The jth row of the **Helmert sub-matrix** H is given by

$$(h_j, ..., h_j, -jh_j, 0, ..., 0), \quad h_j = -\{j(j+1)\}^{-1/2}$$

and so the jth row consists of h_j repeated j times, followed by jh_j and then k-j-1 zeros, j=1,…,k-1.

For k=3 the full Helmert matrix is explicitly

$$H^F = \begin{bmatrix} 1/\sqrt{3} & 1/\sqrt{3} & 1/\sqrt{3} \\ -1/\sqrt{2} & 1/\sqrt{2} & 0 \\ -1/\sqrt{6} & -1/\sqrt{6} & 2/\sqrt{6} \end{bmatrix}$$

and the Helmert sub-matrix is

$$H = \begin{bmatrix} -1/\sqrt{2} & 1/\sqrt{2} & 0 \\ -1/\sqrt{6} & -1/\sqrt{6} & 2/\sqrt{6} \end{bmatrix}.$$

Definition 5.4 The size-and-shape of a configuration matrix X is all the geometrical information about X that is invariant under location and rotation (rigid-body transformations), and this can be represented by the set $[X]_S$ given by $[X]_S = \{X_H \Gamma : \Gamma \in SO(m)\}$, where X_H=HX.

Definition 5.5 The Procrustes distance d_P is obtained by matching the Helmert coordinates X_{H1} and X_{H2} of X_1 and X_2 as closely as possible over rotations. Thus $d_P(X_1, X_2) = \inf_{\Gamma \in SO(m)} \left\| X_{H1} - X_{H2}\Gamma \right\|$, where inf stands for infimum.

This Procrustes distance represents shape distortion in our formation control task, where X_1 is the configuration matrix for three WMRs in the actual formation, and X_2 is the configuration matrix for three WMRs in the desired formation. Both X_1 and X_2 are 3×3 matrices.

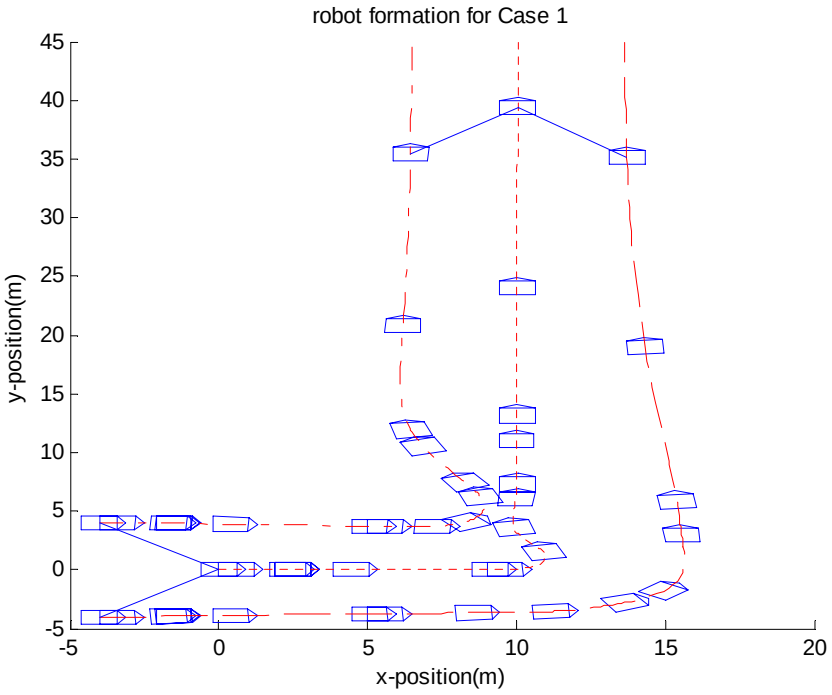

Fig. 5.1 WMR formation in Case I

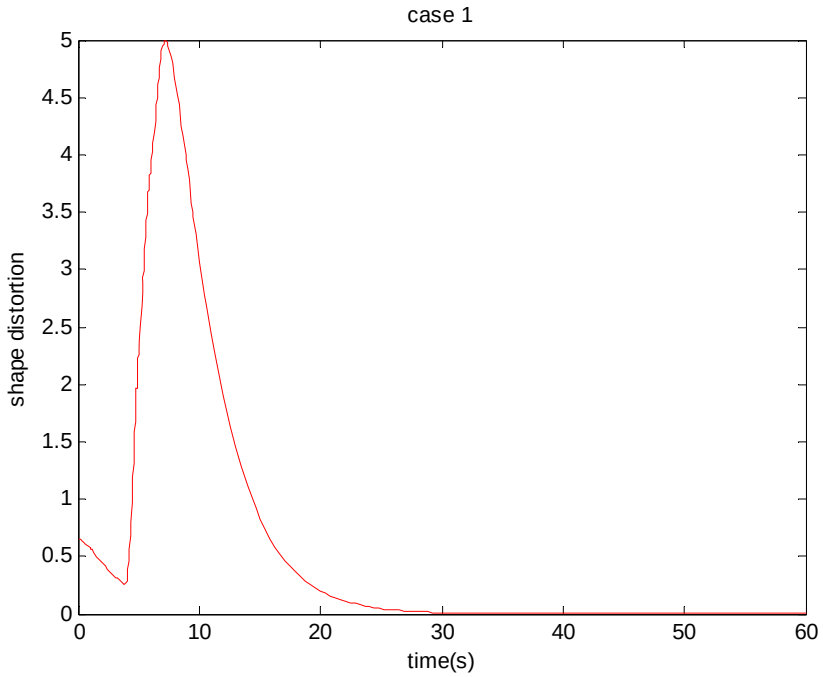

Fig. 5.2 Shape distortion in Case I

Case II: Formation with WMRs having slipping model and no-slipping controller

In this case, everything related to the task is the same as in *Case I* except that each WMR has slipping model. The friction coefficient is 0.3. The triangular formation evolution and shape distortion during *L*-shape path following can be observed in Fig. 5.3 and Fig. 5.4.

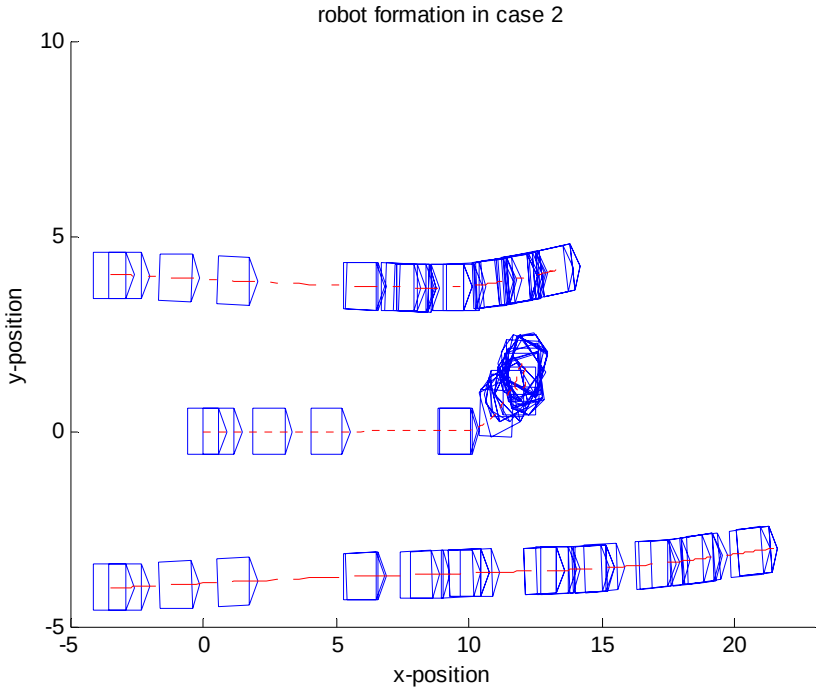

Fig. 5.3 WMR formation in Case II

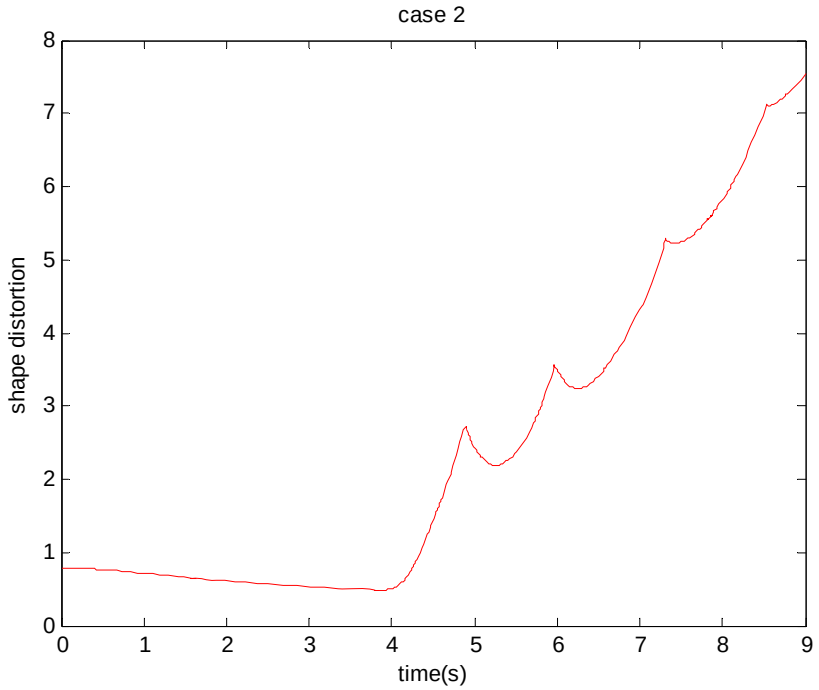

Fig. 5.4 Shape distortion in Case II

Case III: Formation with WMRs having slipping model and slipping controller

In this case, everything related to the task is the same as in *Case II* except for the controllers of the WMRs. Here they all have slipping controllers. In output feedback linearization, we have to take third order derivative of the outputs l and ψ to observe the torque input. The transfer functions for desired l and ψ in the linearized close-loop model are

$$H_{dis}(s) = \frac{K_{p_d}}{s^3 + K_{i_d}s^2 + K_{v_d}s + K_{p_d}}, \qquad H_{ang}(s) = \frac{K_{p_a}}{s^3 + K_{i_a}s^2 + K_{v_a}s + K_{p_a}} \tag{5.2}$$

and the control gains K_{pd}=50, K_{vd}=200.5, K_{id}=102 and K_{pa}=50, K_{va}=200.5, K_{ia}=102, respectively. These control gains are derived by letting the frequency response of the close-loop model in this case same with that in *Case I*. To do so, we need to find a number a>>1 such that

$$(s+a)(s^2 + k_{v_d}s + k_{p_d}) = s^3 + K_{i_d}s^2 + K_{v_d}s + K_{p_d}$$
$$(s+a)(s^2 + k_{v_a}s + k_{p_a}) = s^3 + K_{i_a}s^2 + K_{v_a}s + K_{p_a}.$$

We set a=100, hence K_{pd}=a*k_{pd}=50, K_{vd}=k_{vd}*a+k_{pd}=200.5, K_{id}=a+k_{vd}=102, K_{pa}=a*k_{pa}=50, K_{va}=k_{va}*a+k_{pa}=200.5, K_{ia}=a+k_{va}=102.

The formation evolution and shape distortion during *L*-shape path following can be observed in Fig. 5.5 and Fig. 5.6.

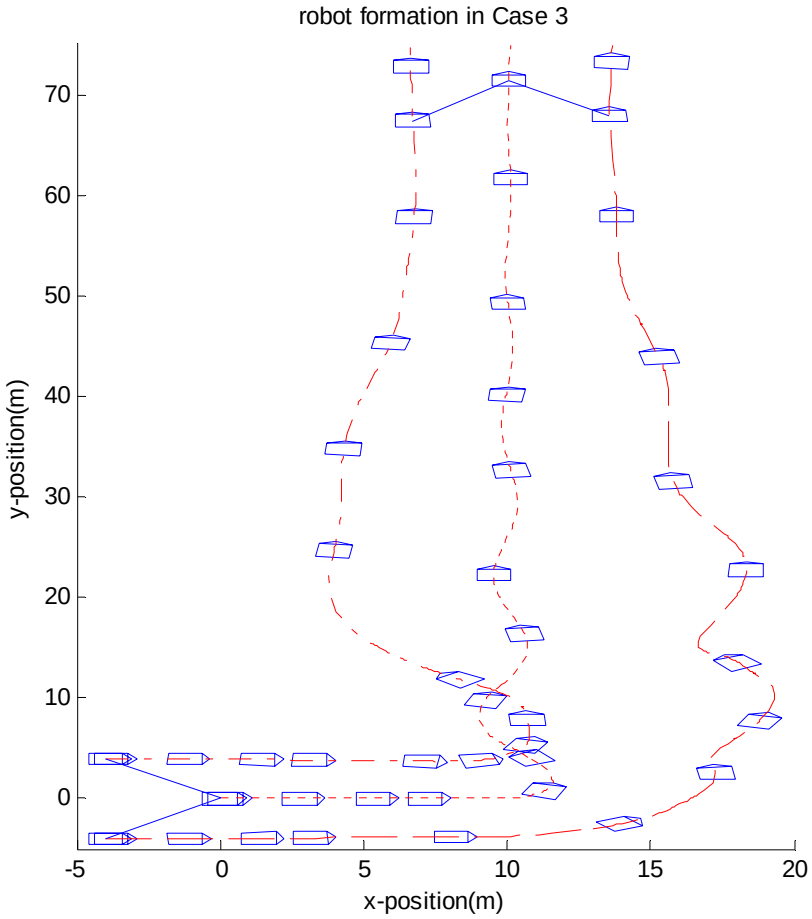

Fig. 5.5 WMR formation in Case III

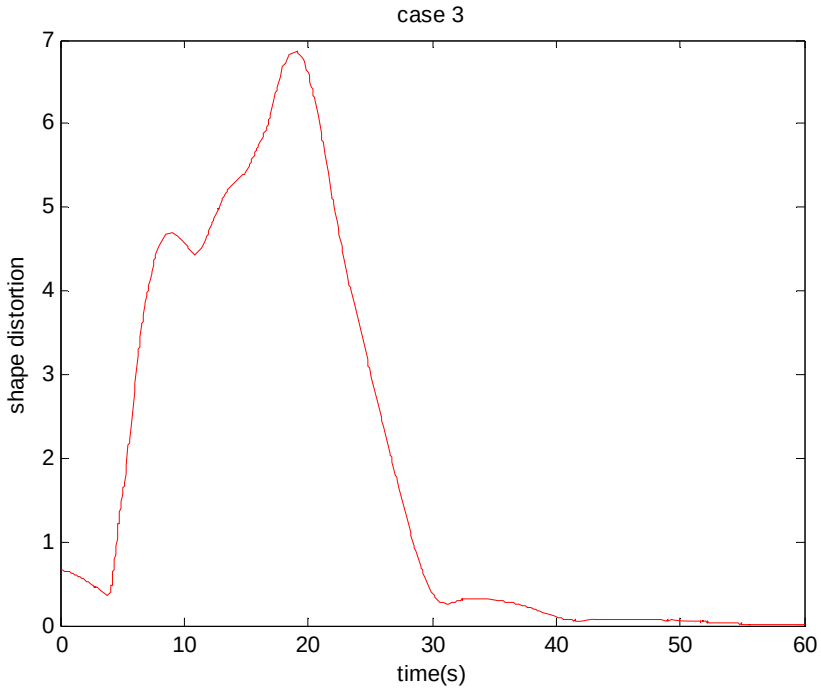

Fig. 5.6 Shape distortion in Case III

CHAPTER VI

APPLICATION III: GAME-BASED PURSUIT-EVASION PROBLEM

From the optimization point of view, P-E problem can be classified into one-sided optimization problem, which is non-game based, and two-sided optimization problem, which is game based. One-sided optimization problem is an optimal control problem where an objective function is optimized for one player, while in two-sided optimization problem an objective function needs to be maximized by one player and to be minimized by the other player simultaneously.

In the literature of non-game-based P-E problems, a randomized pursuer strategy is applied to locate an unpredictable evader and to capture it in a visibility-based P-E problem in [50]. Dynamic programming is applied to find solution in a class of herding problem in [51], and in multi-player P-E problem in [52] where cumulant-based control is used. In [53] nonlinear model predictive controller is applied to an evasive UAV in an aerial P-E problem to help evasion. In [54] a graph theoretic approach is proposed to multi-player P-E problem. In [55] a time-optimal pursuit strategy is proposed in a P-E game and the pursuer takes the worst analysis to capture the evader in a time-efficient and robust fashion even when the evader is intelligent.

Game-based P-E problem is the focus of this dissertation. A game-based P-E problem is a non-cooperative zero-sum game problem for two players, a pursuer and an evader, who have completely opposite interests. The pursuer tries to capture the evader while the

evader tries to avoid being captured. The game arises in numerous situations. Typical examples are search and capture missions, missile guidance to chase an aircraft and aircraft dogfight missions etc.

The first P-E game was the Homicidal Chauffeur game which was studied in 1960s [56]. In this game, the pursuer has higher speed than the evader while the evader does not have turning constraint as the pursuer does. The game is to find regions of initial conditions in game space that guarantee either capture (capture region) or escape (escape region) and to provide optimal strategy for each player. Guaranteed capture means that when the game starts from capture region, no matter what strategy the evader has, there always exists a strategy for the pursuer to achieve capture. Guaranteed escape means that when the game starts from escape region, no matter what strategy the pursuer has, there always exists a strategy for the evader to avoid being captured. The game solution provides the optimal strategy for the pursuer and the evader to follow in order for each to achieve their conflicting goals. Since the evader in the Homicidal Chauffeur game does not have turning constraint, which is not a realistic assumption, the game of two identical cars [57][58] has been studied with both players having turning constraints. In this game it is not possible to solve for the optimal strategy for the two players. In stead, the backward reachable set in the game space is solved for to describe the dependency of the game result on the initial conditions [57]. Capture is guaranteed to occur when the game starts from this set while escape is guaranteed when the game starts from the complement of this set. Generally computation of reachable set is used to verify and validate system design by catching every potential failure mode. Different from simulation, which only

checks a single trajectory of a system each time, reachable set is a way of checking the entire group of trajectories at once. Backward researchable set is a set of all states, starting from which trajectories can reach a given final set of states. In this game the final set of states represents a set of all possible states in the game space at the moment of capture.

In this dissertation, we focus on the two P-E game problems with the pursuer having fully dynamic model subject to wheel slip and we explore new autonomous approaches to the problems. In the Homicidal Chauffeur problem, as a first approach to solve the problem with wheel slip, we present an input-output linearization based feedback controller to compensate for the wheel slip such that capture is still possible. We then present an improved controller that employs extremum seeking control technique to maximize the lateral traction force in the curve segment for the pursuer, in order to minimize the travel in this segment and thus minimize the capture time. We then seek the capture region of the Homicidal Chauffeur game and the backward reachable set of the game of two identical cars. In doing so, we propose a conceptually equivalent kinematic model for the pursuer. Exploring the maximum capability of such a WMR in stable turning motion, we define its equivalent kinematic model as having the same maximum allowed turning curvature at a given speed. We also apply sliding mode-based extremum seeking control technique to practically identify the maximally allowed turning curvature for the WMR. Once such an equivalent model is obtained, the P-E game with the pursuer having fully dynamic model can be reduced to a kinematic P-E game, which will be solved using the algorithms in [56][57]. The solution in [56] gives capture region and

optimal play strategies for the Homicidal Chauffeur game with the equivalent kinematic pursuer. The solution in [57] gives backward reachable set for the game of two identical cars with the equivalent kinematic pursuer.

6.1 Game-based P-E problem without Wheel Slip

6.1.1 Case I: Homicidal Chauffeur game

In the Homicidal Chauffeur game, the pursuer P moves at a fixed speed $v1$, and its radius of curvature is bounded by a given quantity R. It steers by selecting the value of this curvature at each moment. The evader E moves at a fixed speed $v2$ ($v2<v1$) and it steers, at each moment, by choosing its direction of travel. Abrupt changes in this choice are allowed. Each player knows the other's relative location and orientation at each moment. Capture occurs when the distance $PE \le l$, a given quantity. When initial conditions are given in the capture region, the optimal play strategy for each player can be obtained as shown in [56].

To solve this game, individual kinematics equations for two players are integrated into 2-D kinematics represented in terms of the evader's relative location to the pursuer, i.e., the evader's coordinates in game space, which lowers down the number of state variables. The 2-D kinematics in game space is,

$$\begin{aligned} \dot{x} &= -\frac{v_1}{R} y\phi + v_2 \sin\psi \\ \dot{y} &= \frac{v_1}{R} x\phi - v_1 + v_2 \cos\psi \end{aligned} \tag{6.1}$$

where x, y are the evader's coordinates in game space, $|\phi| \le 1$ is the control variable for the

pursuer and ψ is the moving direction of the evader in game space.

It has been proved in [56] that if the following inequality (6.2) is satisfied, the entire game space is the capture region. However if the inverse of (6.2) is satisfied, only a limited area is the capture region, as shown in Fig. 6.1.

$$\frac{l}{R} > \sqrt{1-(\gamma)^2} + \gamma \sin^{-1}(\gamma) - 1 \tag{6.2}$$

where $\gamma = \frac{v_2}{v_1}$. To take an example of the problem, we let *v*1=2m/s, *v*2=0.5m/s, R=2m, and *l*=0.5m.

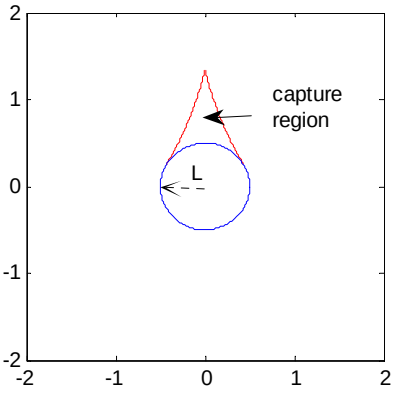

Fig. 6.1. Capture region for the case where (6.2) is not satisfied. The circle is where capture occurs.

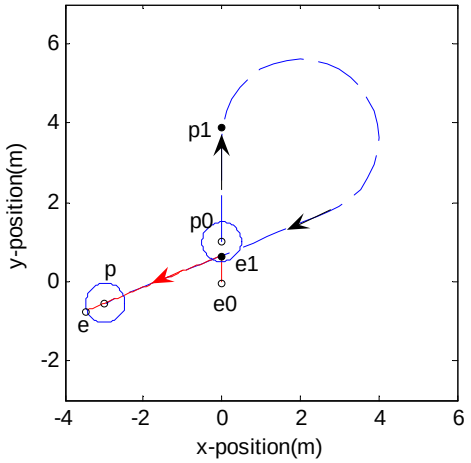

Fig. 6.2 Pursuit evasion paths in Homicidal Chauffeur game: red line is evader's path; blue curve is pursuer's path.

Since (6.2) is satisfied, the entire game space is the capture region. In addition, we assume the evader is initially right behind the pursuer within a short distance, as located at e_0=[0,0] and p_0=[0,1,$\frac{\pi}{2}$] in Fig. 6.2. Under optimal play, the pursuer first goes away from the evader, enlarges the distance in between until the pursuer reaches p_1 and the evader reaches e_1 simultaneously, then makes a turn and goes straight to the evader; while the evader at first follows the pursuer to e_1 and then escapes from it after the pursuer reaches p_1. More details on deriving the optimal play strategies are omitted as they are elaborated in [56].

6.1.2 Case II: Game of Two Identical Cars

In the game of two identical cars, the pursuer P and the evader E have fixed speed v_1 and v_2, respectively, and their radii of curvature are bounded by given quantities R_1 and R_2, respectively. They steer by selecting the value of their curvatures at each moment. Each player knows the other's relative location and orientation at each moment. Capture occurs if two cars come within distance l of one another. However, it is indicated in [58] that only given the initial conditions, the optimal play for the two players can not be derived. In stead, the backward reachable set in the game space is the alternative to study the P-E behavior.

To solve this game, 3-D kinematics in game space is established as

$$\begin{aligned} \dot{x} &= -v_1 + v_2\cos\psi + \omega_1 y \\ \dot{y} &= v_1\sin\psi - \omega_1 x \\ \dot{\psi} &= \omega_2 - \omega_1 \end{aligned} \quad , \tag{6.3}$$

where x, y are the evader's coordinates in game space, ω_1, ω_2 are angular velocities for P and E, respectively, and ψ is the moving direction of the evader in game space.

Take an example of this game from [57], where *v*1=*v*2=5m/s, R1=R2=5m, ***l***=5m and $|\omega_i| \le \frac{v_i}{R_i} = 1\text{m/s}$. The calculated backward reachable set using the toolbox in [59] is shown in Fig. 6.3, where x, y, phi represent the coordinates of the evader relative to the pursuer. The backward reachable set will be larger for $|\omega_1|$ with larger upper bound while smaller for $|\omega_1|$ with smaller upper bound. Additionally, when P starts from p0=[0,0,0] and E starts from e0=[6,-11, $\frac{\pi}{2}$], meaning that the initial state is in the backward reachable set, the pursuit evasion paths are shown in Fig. 6.4 where the pursuer takes pure pursuit [60] strategy, in which the pursuer tries to point its head directly towards the evader, and the evader tries to move away from the evader to maximize the distance.

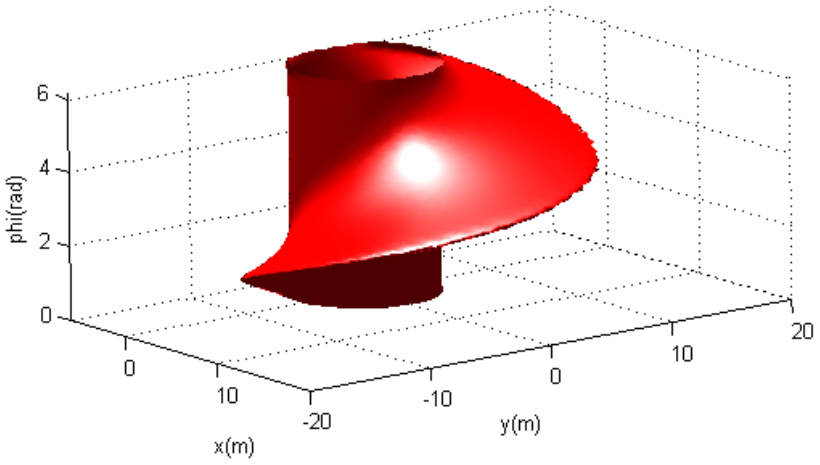

Fig. 6.3 Backward reachable set when v_1=v_2=5, R_1=R_2=5, *l*=5 and $|\omega_1| = |\omega_2| \le 1$

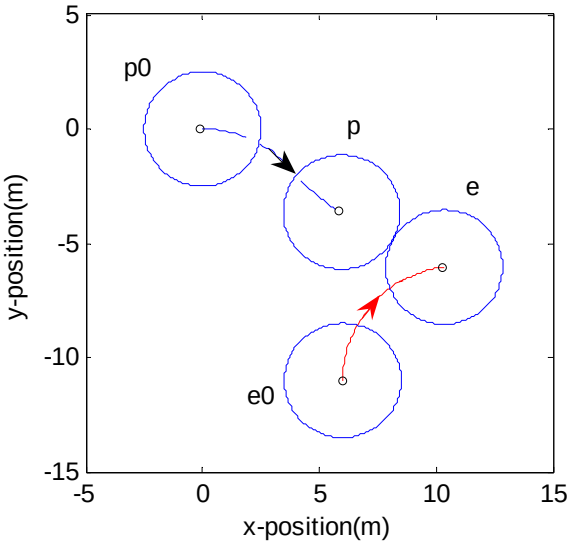

Fig. 6.4 Pursuit evasion paths in the game of two identical cars: red line is the evader's path; dashed blue curve is the pursuer's path.

The optimal play and the backward reachable set need to be solved for the Homicidal Chauffeur game and the game of two identical cars, respectively. The value function of a game is defined as the cost of a trajectory that starts at initial state, evolves with inputs and ends at the final state. Note that we are only interested in whether or not capture occurs, therefore there is only terminal cost and no running cost. The pursuer selects its control action that tries to maximize the cost while the evader tries to minimize the cost, which leads to the optimal cost, a saddle solution of the game. This optimal cost corresponds to optimal inputs for both players. The optimal inputs can be derived analytically in the Homicidal Chauffeur game [56]. In the game of two identical cars, the solution to the game can be characterized using Hamilton-Jacobi-Isaacs (HJI) theory. More precisely, the Hamiltonian of the system is the H function shown in (6.4). The inputs that correspond to the optimal Hamiltonian are the optimal inputs. While it is not possible to solve for the optimal inputs, backward reachable set can be solved instead. Let $\dot{x} = f(x, \omega_1, \omega_2)$ be the compact form of (6.3) and $V(x,t)$ be the value function of the

game. It has been shown in [57] that the solution of $V(x,t)$ to the HJI PDE

$$D_t V(x,t) + \min[0, H(x, D_x V(x,t))] = 0 , \tag{6.4}$$

where $H(x, p) = \max_{\omega_1} \min_{\omega_2} p^T f(x, \omega_1, \omega_2)$,

is the boundary of the backward reachable set when t=0. It is difficult to determine the solution to (6.4) either analytically or numerically, however numeric approximation of the solution can be obtained by various techniques. *Viscosity solution* to (6.4) has been proved in [57] to be the value function of the game. A family of algorithms called *level set methods* have been designed to compute approximations to the viscosity solution to (6.4). The Hamiltonian term, time derivation term and special derivation term in (6.4) are computed using Lax-Friedrichs approximation, a second order TVD RK approximation and a fifth order WENO spatial approximation, respectively. For the definition of above techniques, please refer to [57].

6.2 Game-based P-E with Wheel Slip

6.2.1 Slip effect for the Homicidal Chauffeur game

Assuming the pursuer is a WMR subject to wheel slip, we show examples of how wheel slip affects the P-E behavior and what possible approaches to the problem are. One approach to P-E problem on slippery surface is to develop an input-output linearization-based controller that takes into account the WMR model with slip in (2.1). With such a controller the pursuer is trying to constrain itself on the nominal pursuit path indicated by the optimal play strategy in Section 6.1.1, while the evader has the same

kinematics and evasion strategy as in kinematic game. For the straight line segments, we select the orientation ϕ and the forward velocity v of the pursuer as the outputs. For the curve segment, we select its angular velocity and forward velocity as the outputs, linearize the model, design a linear controller, and control the pursuer to track their desired values indicated by optimal play strategy updated at each moment based on current states. When the full model of the pursuer is introduced as in (2.1), the bound of the curvature, which represents the bound of the angular velocity of the wheels, is replaced by the bound of the wheel torque. We want to see how well the pursuer with wheel slip can follow the nominal pursuit path. The desired forward velocity for the pursuer is chosen to be 2m/s. Surface friction coefficient is 0.3 in this case. With the control gains properly selected, simulation result is shown in Fig. 6.5. We observe that the pursuer tries to follow the nominal pursuit path, while compensating the wheel slip, and eventually captures the evader. More details about input-output linearization technique and dynamic path following control applied on the WMR is omitted here as it can be found in [61][2][43].

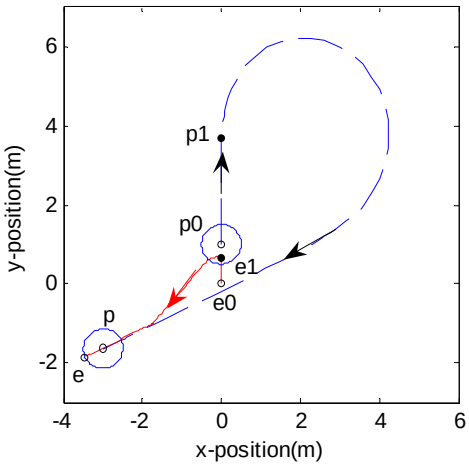

Fig. 6.5 Pursuit evasion paths in the Homicidal Chauffeur game subject to pursuer's wheel slip when friction coefficient is 0.7: red line is evader's path; blue curve is pursuer's path.

In addition, we define a near-optimal solution to the P-E problem in the sense that, the time it takes the pursuer to capture the evader at a constant speed is minimized. Since the pursuit path can be decomposed into straight line and curve segments, to minimize the curve segment is to minimize both the pursuit path and the capture time. In this section, we apply sliding mode-based ESC to maximize the lateral traction force of the pursuer when it is in the curve segment such that this segment is minimized. For straight line segments, we use the same input-output linearization technique to control the same outputs - orientation ϕ and forward velocity v of the pursuer - as discussed above. The evader has the same kinematics and evasion strategy as before. The friction coefficient is 0.3. The P-E paths are shown in Fig. 6.6. It is observed that the pursuer takes a sharp turn to capture the evader, which has better performance than in the first approach. Since the control technique we use in straight line segment is trivial, now we focus on the results in the curve segment, which corresponds to the time from 1.3s to 3.5s. When F_3^r, λ, and α are selected as -57N·m, 0.5, and 0.5, respectively, the actual lateral traction force

moves to its maximum and stays in the small region around the maximum as shown in Fig. 6.7. The maximum of the lateral traction force can be observed in Fig. 2.2. The output of the observer is a very good estimate of the force. However, the lateral traction force for output feedback control case in this duration is far from its maximum. Figure 6.8 is the forward velocity with chatter as it is controlled by sliding mode. In Fig. 6.9 the lateral slip velocity moves to its optimum and stays around it, which corresponds to optimal slip angle, while the lateral slip velocity for the output feedback control case is much less than the optimum. Fig. 6.10 is the angular velocity of each wheel and Fig. 6.11 is the applied torque for each wheel in which we set its bound at 1.24N·m.

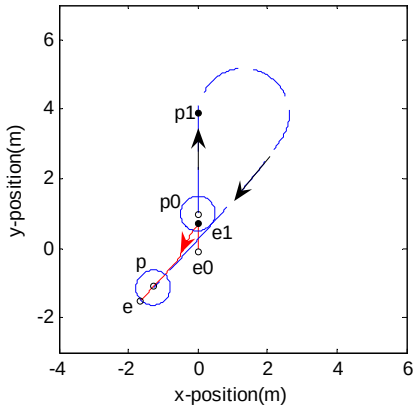

Fig. 6.6 Near-optimal pursuit evasion paths with pursuer on a slippery surface: red line is evader's path; dashed blue curve is pursuer's path.

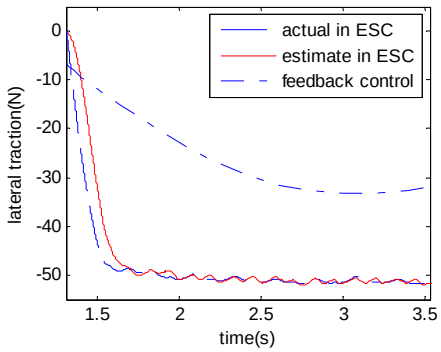

Fig. 6.7 The lateral traction force and its estimate from the observer for ESC in the curve segment, and the lateral traction force for output feedback control in the same time window.

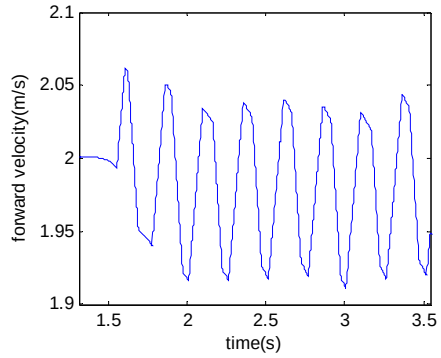

Fig. 6.8 WMR forward velocity in the curve section

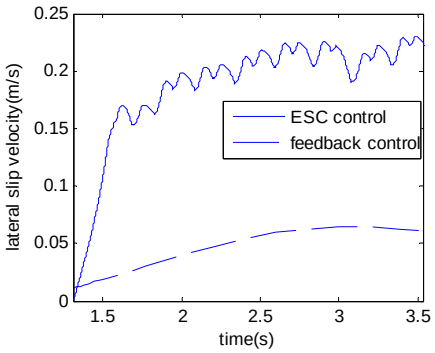

Fig. 6.9 Lateral slip velocity for ESC in the curve segment, and lateral slip velocity for output feedback control in the same time window.

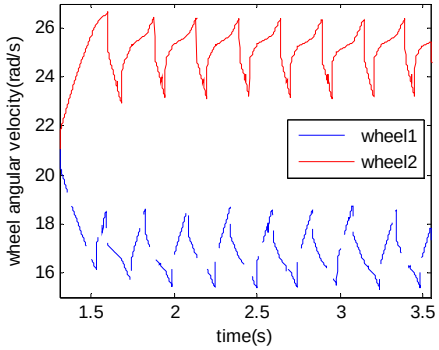

Fig. 6.10 Wheel angular velocity in the curve section.

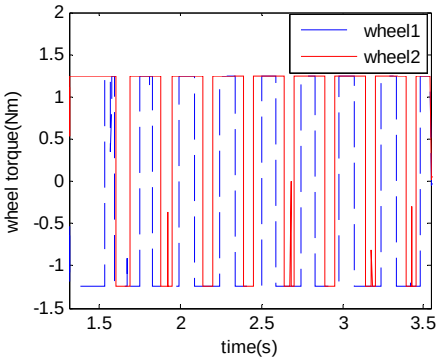

Fig. 6.11 Wheel torque in the curve section.

We simulate the problem in Fig. 6.12 in which capture does not occur when the friction coefficient is 0.1. In this simulation, initial conditions are the same as in Section 6.1.1 except that $v1$=1m/s. Note that when the pursuer starts to make a turn, the instant curvature indicates that the game is in escape region, so that the evader does not have to move right away and still can avoid capture by moving sidewise when the pursuer approaches close enough. Note that in Fig. 6.12 when P is at p1 and E is at e1 they have the shortest distance from each other. This simulation shows that even with slip-based controller, capture still may not happen.

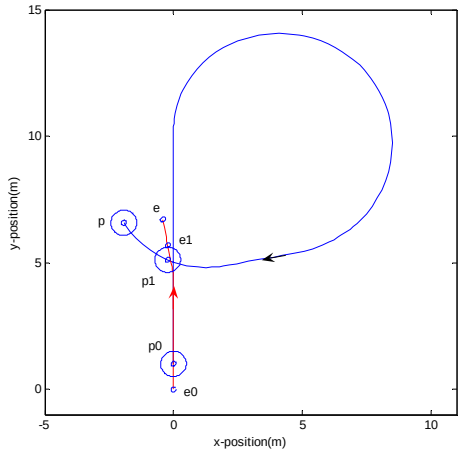

Fig. 6.12 Pursuit evasion paths in the Homicidal Chauffeur game subject to pursuer's wheel slip when friction coefficient is 0.1: red line is evader's path; blue curve is pursuer's path.

6.2.2 Slip effect for the game of two identical cars

In the game of two identical cars, we simulate the problem in Fig. 6.13-6.14 in which capture occurs when the friction coefficient is 0.7 while does not occur when the friction coefficient is 0.1. Note that in Fig. 6.14 when P is at p_1 and E is at e_1 they have the shortest distance from each other.

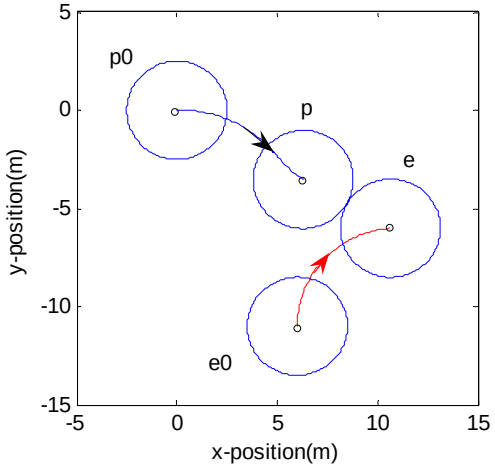

Fig. 6.13 Pursuit evasion paths in the game of two identical cars subject to pursuer's wheel slip when friction coefficient is 0.7: red line is evader's path; blue curve is pursuer's path.

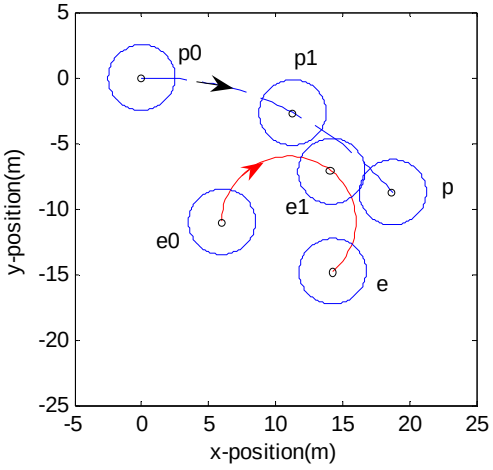

Fig. 6.14 Pursuit evasion paths in the game of two identical cars subject to pursuer's wheel slip when friction coefficient is 0.1: red line is evader's path; blue curve is pursuer's path.

It is shown in the above example that the introduction of wheel slip may break the rule that governs the behavior of the players in a P-E game. Therefore we want to find a solution to the game when fully dynamic model and wheel slip are introduced. If a game system has a fully dynamic model, the model can be transformed into a higher dimensional system of first order ODEs and treated as a kinematic model such that the algorithms in [57] can be applied to solve the HJI equation. The highest dimension that has been observed in the literature is four as in the aircraft landing example [62], where the computation takes several days. However, as the dimension becomes larger, the algorithms become computationally infeasible [63]. For example in the game of two identical cars, if the pursuer has a fully dynamic model subject to wheel slip, the model can be transformed to a system of nine dimension, which makes the computation extremely time consuming. Therefore, we want to simplify the problem by certain approximation. Physical behavior of the WMR pursuer subject to wheel slip is studied. Based on the behavior level approximation we propose a conceptually equivalent kinematic model for P-E game such that the algorithms in [57] can be applied.

6.3 Equivalent Kinematic Model for the Dynamic WMR Subject to Wheel Slip

6.3.1 Equivalent Kinematic Model

In this section, a kinematic model is defined to be equivalent to a dynamic WMR subject to wheel slip if its lower bound of the radius of curvature is the same as the dynamic model's minimum allowed radius of curvature in stable motion at a given speed.

For the dynamic WMR, it has been shown in [29][30] that the slip dynamics is open loop unstable when the WMR operates at wheel slip values to the right of the peak of the friction curve. Thus when seeking the equivalent kinematic model, we require the dynamic WMR to operate always at the wheel slip values to the left of the peak of the friction curve.

Minimum allowed radius of curvature at a given speed:

When the WMR takes a turn at constant forward and angular velocity, the resultant tangential force is zero, the resultant normal force entirely contributes to the centripetal acceleration, and the resultant external moment is zero. For kinematic model, it is assumed that the normal force can be as much as needed for turning. Thus the radius of curvature can be theoretically arbitrarily small. However for the dynamic WMR subject to wheel slip, the dynamics is governed by (6.5) where the normal force is limited by traction forces.

$$\begin{aligned} \sum F_t &= (F_1 + F_2)\cos\theta - F_3 \sin\theta = 0 \\ \sum F_n &= (F_1 + F_2)\sin\theta + F_3 \cos\theta = M\,\frac{v^2 + \dot{\eta}^2}{R} \\ \sum M &= (F_1 - F_2)r - F_3 d = 0 \end{aligned} \tag{6.5}$$

Assume both the optimal lateral slip velocity $\dot{\eta}_{opt}$ and the corresponding maximum lateral traction force are known, for given forward speed *v*, the minimum allowed radius of curvature is

$$R = \frac{M(v^2 + \dot{\eta}_{opt}{}^2)\cos\theta}{\max(F_3)} \quad \text{where} \quad \tan(\theta) = \frac{\dot{\eta}_{opt}}{v}. \tag{6.6}$$

Since F3 is a function of $\dot{\eta}_{opt}$ and *v*, *R* is a function of $\dot{\eta}_{opt}$ and *v*. To control the WMR to imitate its equivalent kinematic model, we apply input-output linearization technique to control its forward velocity and angular velocity to track the given forward

velocity and the maximum allowed angular velocity from (6.6), respectively.

6.3.2 Control Approach to Determine Minimum Allowed Radius of Curvature

This approach is introduced in Section 3.2, where the minimum turning radius of the WMR model is derived by controlling the WMR to make a sharpest possible turn. Sliding mode based extremum seeking technique is applied to control the lateral traction force to maintain at its maximum during turning. The radius of curvature derived here is more practical as it comes from real experiment. Since both radii of curvature obtained in Section 6.3.1 and 6.3.2 correspond to maximum lateral traction, they are approximately equal to each other for the same surface characteristic. However, it has been shown in [44] that this sliding mode-based approach enables the lateral traction force to converge faster to its maximum than the optimal slip tracking control.

6.4 Capture Region and Backward Reachable Set of the P-E Games with the Equivalent Kinematic Pursuer

In this section, we show the equivalent kinematic model of the dynamic WMR pursuer at various speeds on surfaces with various characteristics. Using the equivalent kinematic models, we show the capture region for the Homicidal Chauffeur game and the backward reachable set for the game of two identical cars.

6.4.1 Equivalent Kinematic Model of the Dynamic WMR Pursuer

TABLE I

EQUIVALENT KINEMATIC MODEL FOR DYNAMIC WMR

Velocity (m/s)	Friction Coefficient	Max (F_3) (N)	$\dot{\eta}_{opt}$ (m/s)	Radius of Curvature (m)
1	0.1	17.6	0.18	1
1	0.3	53	0.18	0.3
2	0.1	17.6	0.36	3.9
2	0.3	53	0.36	1.3
3	0.1	17.6	1.1	8.8
3	0.3	53	1.1	2.9

Let the maximum allowed speed of the WMR be 3m/s. At this speed, when the friction coefficient is 0.3 and the lateral traction force is as defined in (2.6), it is seen from (6.6) and Fig. 2.2 that the minimum radius of curvature is R=2.9m, where M=17kg. For more speed and friction coefficient options, the equivalent kinematic models are shown in Table I.

6.4.2 Capture Region in the Homicidal Chauffeur Game with Equivalent Kinematic Pursuer

For the game with dynamic WMR pursuer, given $v1$ and $v2$, when (6.6) is substituted into (6.2), the entire game space is the capture region if (6.7) is satisfied and on the other hand the capture region is a limited area in the game space if (6.7) is not satisfied.

$$\frac{l\max(F_3)}{M(v_1^{\,2}+\dot{\eta}_{opt}^{\,2})\cos\theta} > \sqrt{1-(\gamma)^2}+\gamma\sin^{-1}(\gamma)-1 \quad \text{where} \quad \tan(\theta)=\frac{\dot{\eta}_{opt}}{v_1} \tag{6.7}$$

Assuming $v2$=0.5m/s and l=0.24m, which is the WMR's radius, for all the cases in Table I for the pursuer, the entire game space is the capture region. However, when we select higher $v2$, e.g., $v2$=1.5m/s, then for the cases where $v1$=2m/s and friction coefficient is 0.3, the capture region is a limited area as shown in Fig. 6.15.

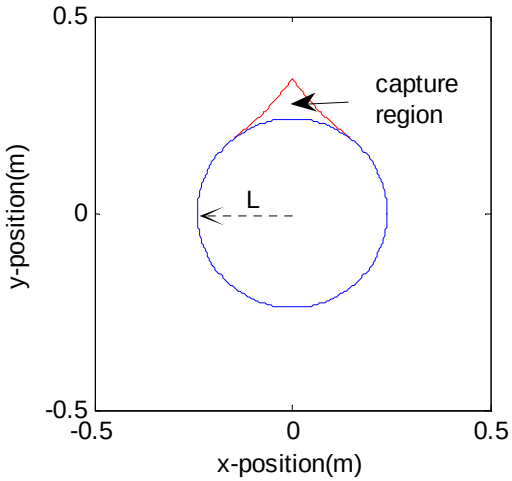

Fig. 6.15 Capture region for the case where (22) is not satisfied. The circle is where capture occurs.

6.4.3 Backward Reachable Set in the Game of Two Identical Cars with Equivalent Kinematic Pursuer

In this game, we take two examples with two different pursuers from Table I where ***v***1=2m/s, friction coefficient=0.3 and ***v***1=3m/s, friction coefficient=0.1, respectively. In the first example, the corresponding R1=1.3m and we take ***v***2=2m/s, R2=2m, $|\omega_2| \le \frac{v_2}{R_2} = 1$, *l*=0.48m. The backward reachable set is shown in Fig. 6.16. In the second example, the corresponding R_1=8.8m and we take the same parameters for the evader as in last example. The backward reachable set is shown in Fig. 6.17.

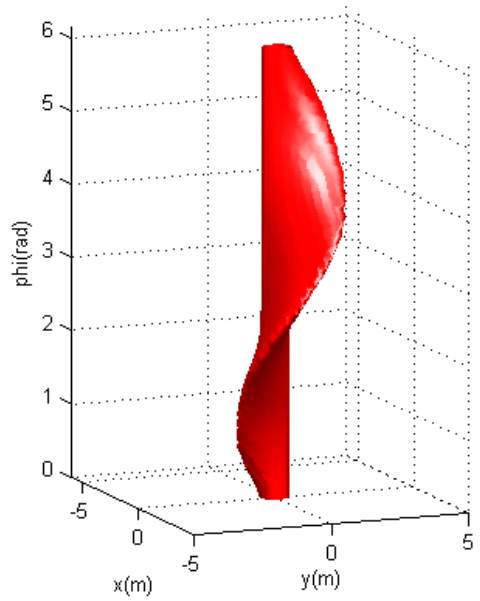

Fig. 6.16 Backward reachable set when $v_1=v_2=2$m/s, $R_1=1.3$m, $R_2=2$m, $l=0.48$m, $|\omega_2| \le 1$, $|\omega_1| \le 1.54$

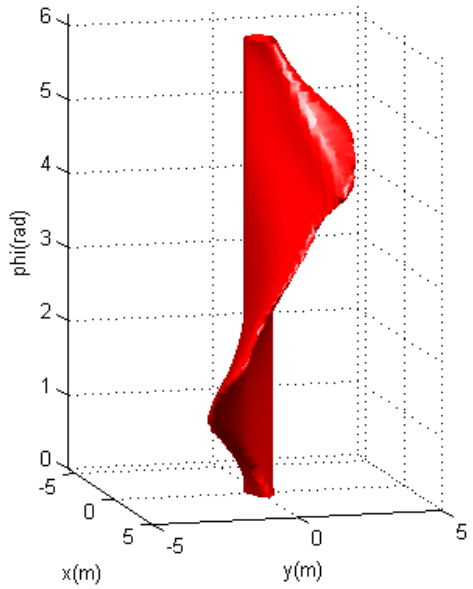

Fig. 6.17 Backward reachable set when $v_1=3$m/s, $v_2=2$m/s, $R_1=8.8$m, $R_2=2$m, $l=0.48$m, $|\omega_2| \le 1$, $|\omega_1| \le 0.34$.

6.5 Simulation Results

We verify the capture region and the backward reachable set for the reduced P-E game by selecting the WMR pursuer subject to wheel slip and its equivalent kinematic model, applying a general pursuit strategy, selecting initial conditions from inside the capture region or the backward reachable set, and simulating the capture scenario. We can also simulate the escape scenario by selecting initial conditions from outside the capture region or the backward reachable set. By comparing the behavior of the dynamic WMR pursuer and its equivalent kinematic model, we verify the equivalence by seeing insignificant difference between them.

6.5.1 Homicidal Chauffeur game with the WMR pursuer subject to wheel slip and its equivalent kinematic model

We take a capture and an escape scenario from the examples in Section 6.2. First we take $v1$=1m/s, friction coefficient=0.3, equivalent R1=0.3m, $v2$=0.5m/s and l=0.24m. It has been shown that in this case the entire game space is the capture region. In Fig. 6.18, Fig. 6.19 and Fig. 6.20, we select initial positions as p0=[0,0,0] and e0=[2,0]. When pure pursuit strategy is applied to the pursuer, and the evader moves along a sinusoidal trajectory, the simulations show the capture scenario for both the WMR pursuer subject to wheel slip and its equivalent kinematic pursuer. We notice that the pursuit and evasion paths in these two figures are very close to each other. Then we take $v1$=2m/s, friction coefficient=0.3, equivalent R1=1.3m, $v2$=1.5m/s and l=0.24m. It has been shown in Fig. 6.15 that when the two players start with a distance far enough in between, the game is in escape region. We select the initial positions as p0=[0,0,0] and e0=[0.5,0]. Fig. 6.21, Fig. 6.22 and Fig. 6.23 show the escape scenario for both the WMR pursuer subject to wheel slip and its equivalent kinematic pursuer when pure pursuit is applied to the pursuer. Note that in these two figures, when P is at p1 and E is at e1, they come within the shortest distance of each other, while either before or after that the distance is larger. When P comes back to E again after a wide turn, E can avoid capture using the same moving strategy.

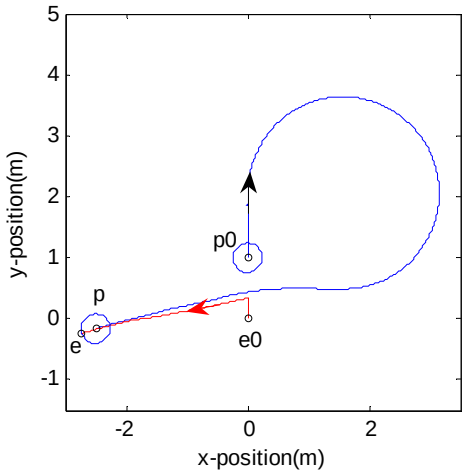

Fig. 6.18(a). Capture scenario for dynamic WMR pursuer subject to wheel slip governed by velocity tracking control.

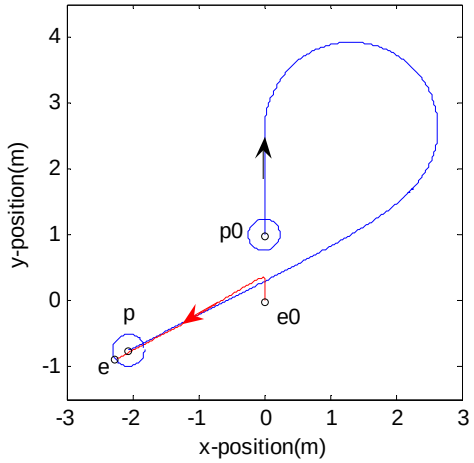

Fig. 6.19(a). Capture scenario for dynamic WMR pursuer subject to wheel slip governed by sliding-mode based extremum seeking control technique.

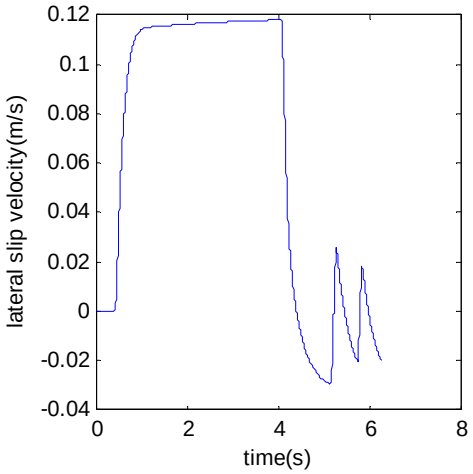

Fig. 6.18(b). Lateral slip velocity for dynamic WMR pursuer subject to wheel slip governed by velocity tracking control.

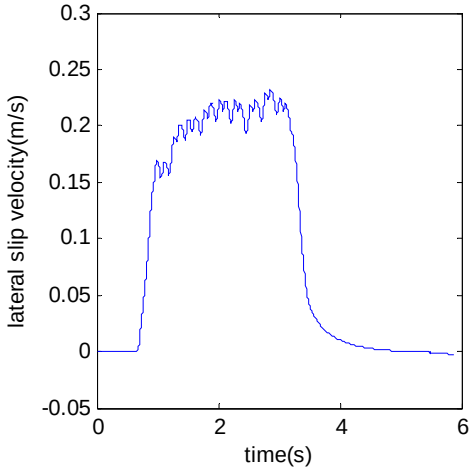

Fig. 6.19(b). Lateral slip velocity for dynamic WMR pursuer subject to wheel slip governed by sliding-mode based extremum seeking control technique.

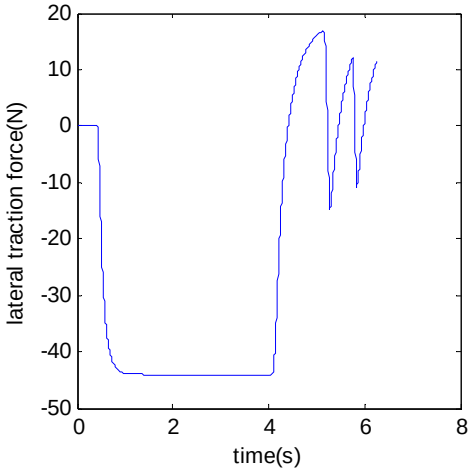

Fig. 6.18(c). Lateral traction force for dynamic WMR pursuer subject to wheel slip governed by velocity tracking control.

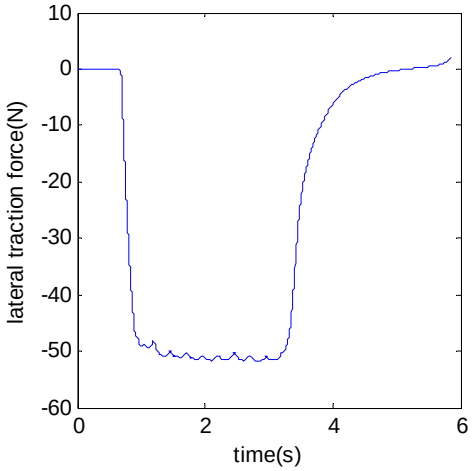

Fig. 6.19(c). Lateral traction force for dynamic WMR pursuer subject to wheel slip governed by sliding-mode based extremum seeking control technique.

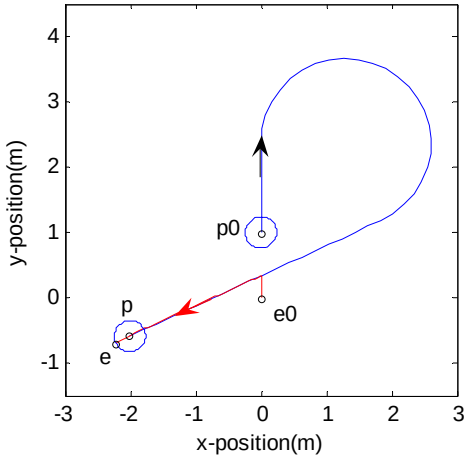

Fig. 6.20. Capture scenario for equivalent kinematic pursuer

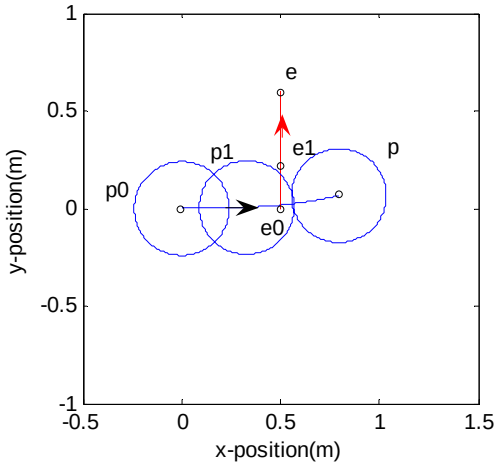

Fig. 6.21(a). Escape scenario for dynamic WMR pursuer subject to wheel slip governed by velocity tracking control

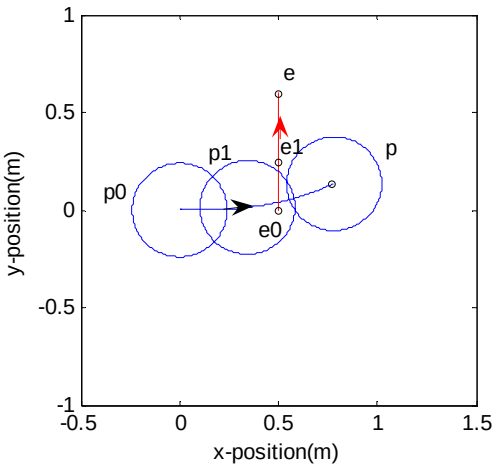

Fig. 6.22(a). Escape scenario for dynamic WMR pursuer subject to wheel slip governed by sliding-mode based extremum seeking control technique.

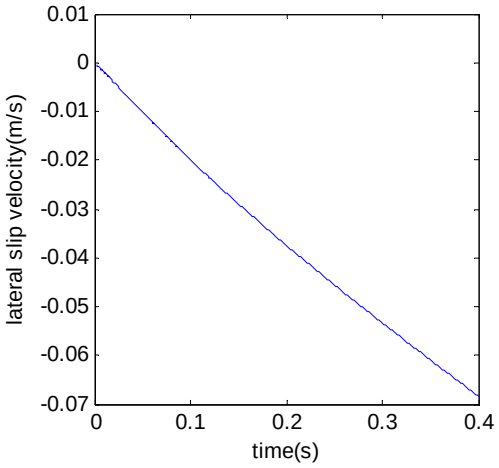

Fig. 6.21(b). Lateral slip velocity for dynamic WMR pursuer subject to wheel slip governed by velocity tracking control

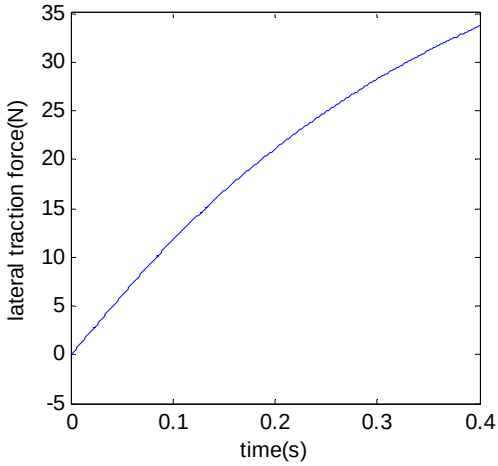

Fig. 6.21(c). Lateral traction force for dynamic WMR pursuer subject to wheel slip governed by velocity tracking control.

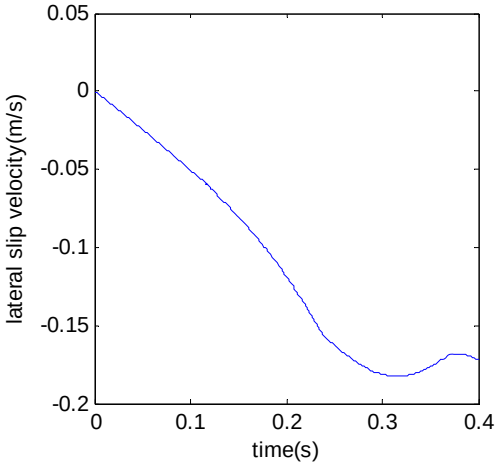

Fig. 6.22(b). Lateral slip velocity for dynamic WMR pursuer subject to wheel slip governed by sliding-mode based extremum seeking control technique.

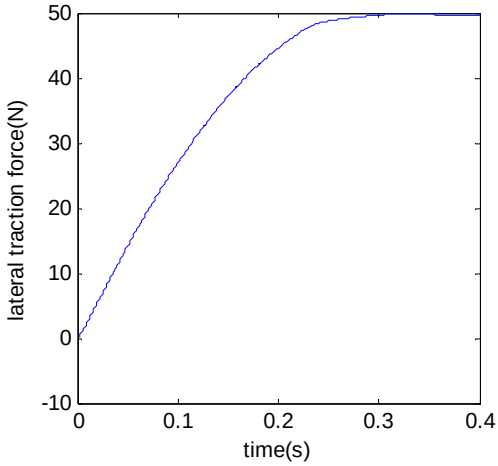

Fig. 6.22(c). Lateral traction force for dynamic WMR pursuer subject to wheel slip governed by sliding-mode based extremum seeking control technique.

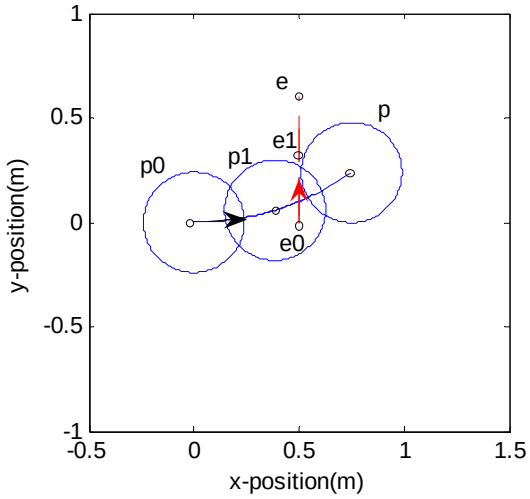

Fig. 6.23. Escape scenario for equivalent kinematic pursuer

6.5.2 The game of two identical cars with the WMR pursuer subject to wheel slip and its equivalent kinematic model

We take a capture and an escape scenario from the examples in Section 6.3. We take $v1$=2m/s, friction coefficient=0.3, equivalent R1=1.3m, $v2$=2m/s, R2=2m and l=0.48m. We select initial conditions from inside and outside the backward reachable set in Fig. 6.16, respectively. For the initial conditions inside the backward reachable set, We select initial position as p0=[0,0,0] and e0=[3,0,π]. Fig. 6.24, Fig. 6.25 and Fig. 6.26 show the

capture scenario for both WMR pursuer subject to wheel slip and its equivalent kinematic pursuer, when pure pursuit is applied to the pursuer. For the initial conditions outside the backward reachable set, We select initial position as p0=[0,0,0] and e0=[5,0, π]. Fig. 6.27, Fig. 6.28 and Fig. 6.29 show the escape scenario for both WMR pursuer subject to wheel slip and its equivalent kinematic pursuer, when pure pursuit is applied to the pursuer. Note that when P is at p1 and E is at e1 in Fig. 6.27 and Fig. 6.28, and when P is at p and E is at e in Fig. 6.29, the two players come within the shortest distance of each other. After P reaches p and E reaches e, the two players are moving along the same direction and capture will never happen as long as E is moving straight.

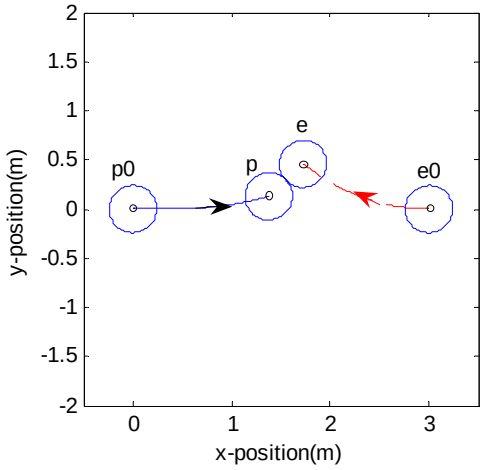

Fig. 6.24(a). Capture scenario for dynamic WMR pursuer subject to wheel slip governed by velocity tracking control

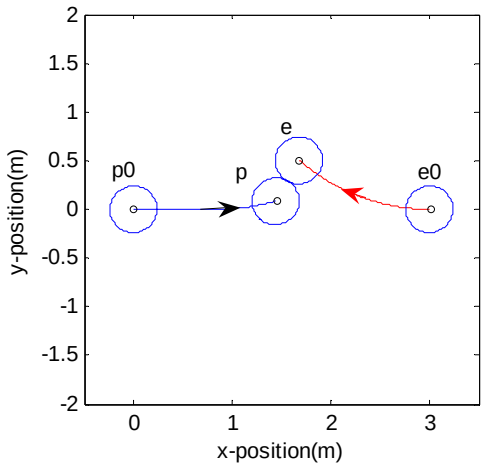

Fig. 6.25(a). Capture scenario for dynamic WMR pursuer subject to wheel slip governed by sliding-mode based extremum seeking control technique.

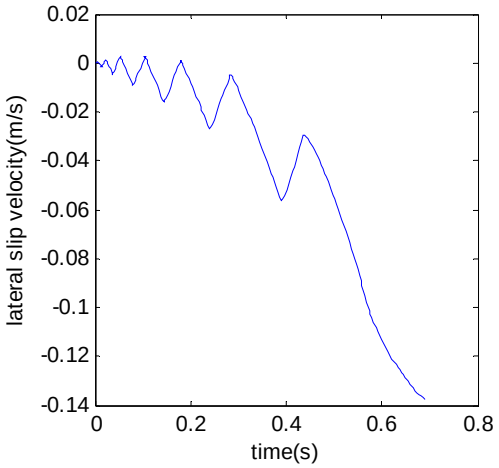

Fig. 6.24(b). Lateral slip velocity for dynamic WMR pursuer subject to wheel slip governed by velocity tracking control.

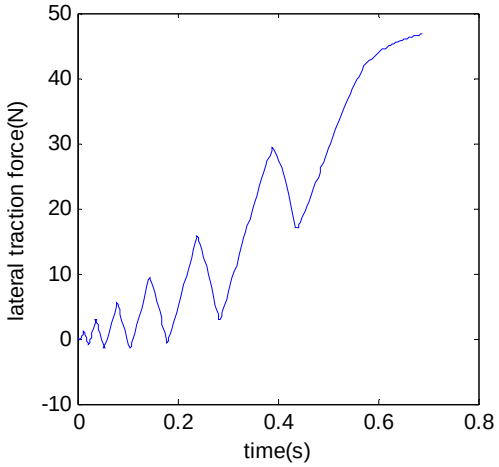

Fig. 6.24(c). Lateral traction force for dynamic WMR pursuer subject to wheel slip governed by velocity tracking control.

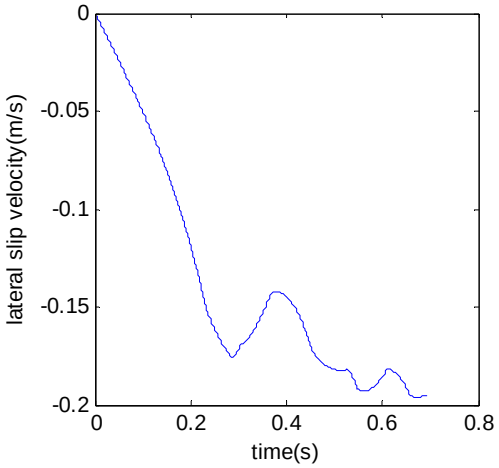

Fig. 6.25(b). Lateral slip velocity for dynamic WMR pursuer subject to wheel slip governed by sliding-mode based extremum seeking control technique.

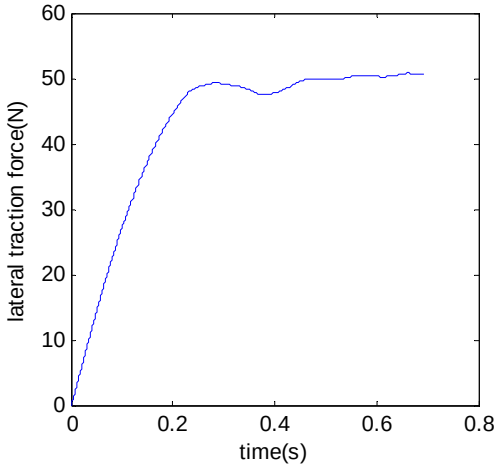

Fig. 6.25(c). Lateral traction force for dynamic WMR pursuer subject to wheel slip governed by sliding-mode based extremum seeking control technique.

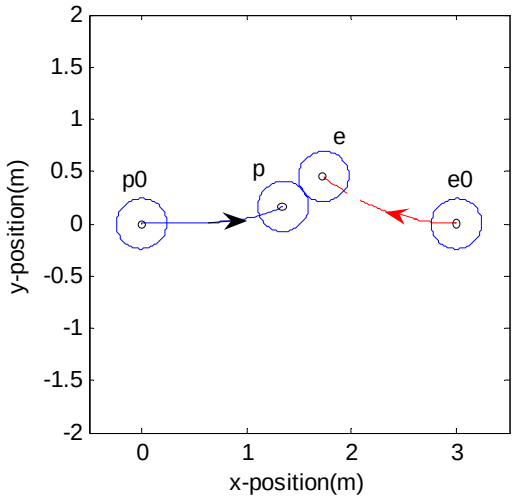

Fig. 6.26. Capture scenario for equivalent kinematic pursuer

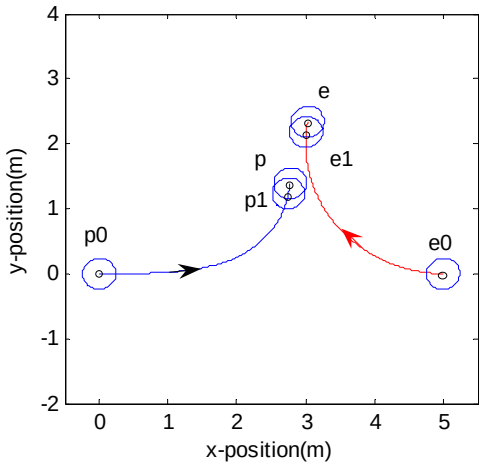

Fig. 6.27(a). Escape scenario for dynamic WMR pursuer subject to wheel slip governed by velocity tracking control

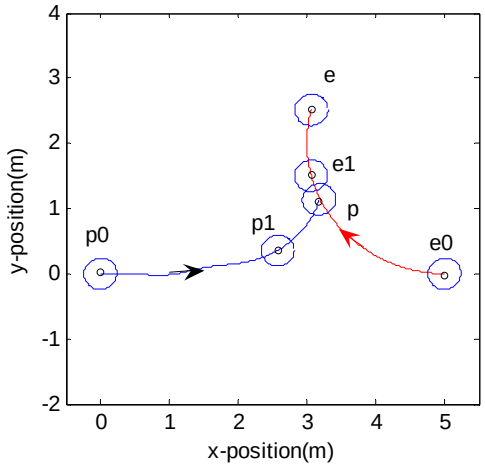

Fig. 6.28(a). Escape scenario for dynamic WMR pursuer subject to wheel slip governed by sliding-mode based extremum seeking control technique.

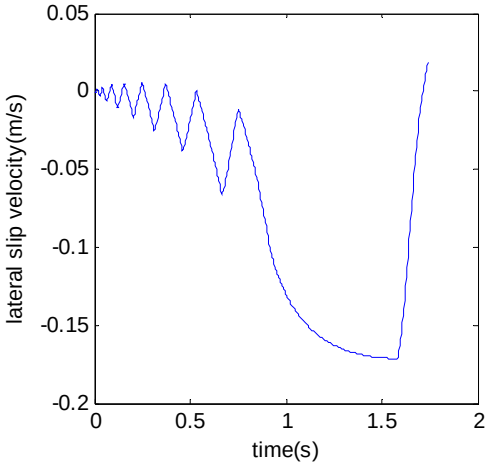

Fig. 6.27(b). Lateral slip velocity for dynamic WMR pursuer subject to wheel slip governed by velocity tracking control.

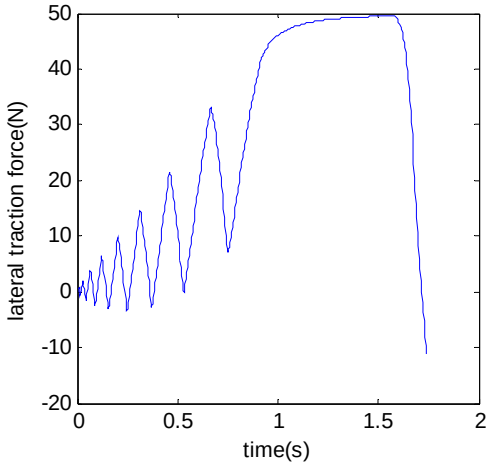

Fig. 6.27(c). Lateral traction force for dynamic WMR pursuer subject to wheel slip governed by velocity tracking control.

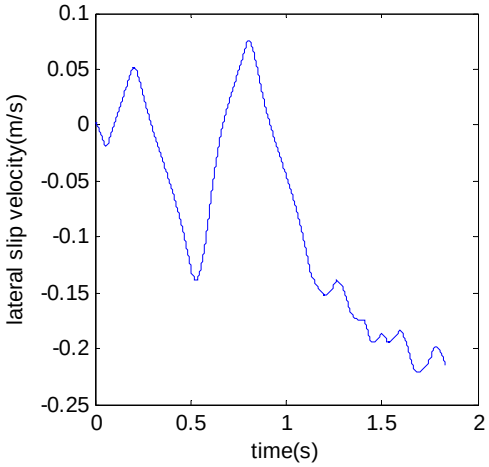

Fig. 6.28(b). Lateral slip velocity for dynamic WMR pursuer subject to wheel slip governed by sliding-mode based extremum seeking control technique.

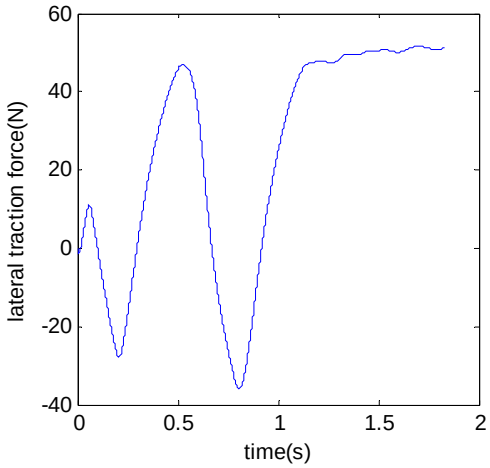

Fig. 6.28(c). Lateral traction force for dynamic WMR pursuer subject to wheel slip governed by sliding-mode based extremum seeking control technique.

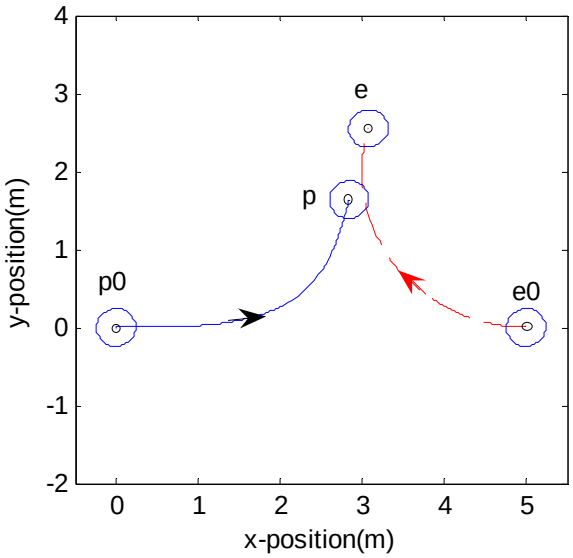

Fig. 6.29. Escape scenario for equivalent kinematic pursuer

CHAPTER VII

CONTRIBUTIONS AND FUTURE WORK

7.1 Contributions

In this dissertation, we investigate the effect of wheel slip on the control problems of a nonholonomic WMR and present a framework that can control a WMR in the presence of wheel slip. We then apply this framework to several single WMR applications (i.e., regulation, tracking, path following, sharp turning) and multi-WMR applications (i.e., formation control and game-based P-E problem). There are several contributions of this research that span both theory and applications.

First, we model the dynamics of a WMR subject to both longitudinal and lateral wheel slips. This model integrates the WMR main body dynamics, wheel spinning dynamics, nonholonomic constraints and traction force model into a combined compact dynamic model in the world coordinates. This model is different from ideal models of nonholonomic WMRs [2] in that it introduces slip constraints and traction force model into the overall dynamics, which allows more realistic interaction with the environment. This model is also different from other models with slip constraints in that in those models either the slip is considered as a perturbation to the WMR dynamics [3][4][6], or a nonlinear traction force model is not considered in control design so that the effect of traction forces to the WMR due to variation of slip can be investigated [7][8]. The model in this dissertation is one of the first attempts that properly models wheel slips, captures

the nonlinear effect of traction forces to the control of a nonholonomic WMR, and enables control of positions, velocities and traction forces for the WMR.

Second, we investigate the effect of wheel slip for a single WMR by designing two new controllers and modifying a standard controller for various control problems. We design a σ-process based discontinuous feedback controller for the regulation problem. The introduction of wheel slip transforms the WMR into an underactuated system. Thus all the existing control algorithms for the WMR without slip do not work when slipping is allowed to take place. It has been shown that such a system is not asymptotically stabilizable to a given equilibrium solution using a time-invariant continuous feedback [38]. However, such a system is asymptotically stabilizable to a desired equilibrium using time-variant discontinuous feedback laws. In the literature, the σ-process based discontinuous control law has been developed for the control of a surface vessel, a typical underactuated system modeled in local coordinates. We transform the dynamics of the WMR into local coordinates and modify this σ-process based discontinuous control law for our WMR model such that the control law can be applied to regulation control of the WMR with slip. This is the first time in the literature that a control law is designed for an underactuated nonholonomic WMR subject to wheel slip to address the regulation control problem. We then modify a standard input-output linearization technique based controller and apply it to tracking control and path following control problems for the WMR to investigate and accommodate the slip effect. This standard controller has been applied to various control problems for WMRs without wheel slip [2]. However, there is no work in the literature that has applied such a controller to a nonholonomic WMR to investigate the

slip effect. We observe the stability in these control problems when the controller that has slip information is applied as well as the instability in these problems when the controller that has no slip information is applied. We then design a sliding mode based ESC that enables the WMR to make the sharpest possible but stable turn, which directly improve the maneuverability of the WMR subject to wheel slip. In the literature the sliding mode based ESC has been designed for ABS of a vehicle to optimize the longitudinal traction forces, without having the knowledge of optimal longitudinal slip and analytic form of the longitudinal traction forces, so that the vehicle can make a stop with highest possible deceleration [32]. In this work, a sliding mode based observer is designed to estimate the longitudinal traction forces using the angular velocity information of the wheels. In this dissertation, we design a sliding mode based ESC to optimize the lateral traction force, without having the knowledge of optimal lateral slip and analytic form of the lateral traction force, so that whenever the WMR needs to make a turn it can make a sharpest possible turn at minimum turning radius without losing stability. Here we design a sliding mode based observer to estimate the lateral traction force using the combined information of the angular velocities for both the wheels and the WMR. This is the first time in the literature that the effect of slip is investigated for turning control problems for a WMR and the maneuverability of the WMR is improved by designing a controller that optimizes the lateral traction force such that the turning radius is minimized.

Third, we investigate the effect of wheel slip for multi-WMR coordination in formation control problems. Formation control is an important area of application for multiple WMRs and many control algorithms have been designed for WMRs without slip

[46][47][48]. However as we have shown in this dissertation, when these formation control algorithms are applied to cases where slip is not negligible (e.g., slippery surface), they tend to fail and the formation is broken. There is no work in the literature to our knowledge that has designed controllers for multiple WMRs to investigate and accommodate the slip effect in formation control problems. We apply the standard input-output linearization technique to design controllers for various formation control problems. We show that by applying a controller that takes slip into consideration, the formation control problem can be stabilized.

Fourth, we investigate the effect of wheel slip for game-based P-E problems. In the literature there are two typical zero-sum game-based P-E problems (i.e., Homicidal Chauffeur game and the game of two identical cars), in which both players have kinematic constraints and have completely opposite interests [56][57]. When slip is introduced into the players, the P-E behavior may change and the rule that governs such a behavior may be inadequate. However, there is no work in the literature that has investigated slip effect for game-based P-E problems. In this dissertation, we assume that the pursuer is a WMR which has wheel slip. We apply input-output linearization technique to design a control law for the pursuer in the Homicidal Chauffeur game to follow the game-based solution updated at each moment based on current kinematic state information, which achieves capture. We then apply the sliding mode based ESC to the pursuer in the Homicidal Chauffeur game such that in the curve segment the pursuer can make a sharpest possible turn and spend minimum time. Therefore the capture performance is improved by minimizing the overall capture time. We then investigate the

P-E behavior by studying the capture region of the Homicidal Chauffeur game and the backward reachable set of the game of two identical cars where the pursuer is subject to wheel slip. Since it is not possible so far to derive an analytic game based solution for the two games, we seek approximated solutions by studying the connections between kinematic games and dynamic games. We study the maximum turning capability of a WMR subject to wheel slip at various speeds. The minimum turning radius at a given speed can be achieved by applying the sliding mode based ESC. Based on this minimum turning radius, we propose a conceptually equivalent kinematic model for the pursuer at a given speed, such that each game can be reformulated to its kinematic form and we can study the P-E behavior by applying the solution to kinematic games. Applying the equivalent kinematic model to the pursuer, we derive the capture region and optimal play strategies for the Homicidal Chauffeur game and the backward reachable set for the game of two identical cars. We show by increasing the friction coefficient of the surface that the capture region and the backward reachable set converge to their kinematic solution and thus validate the concept of kinematic equivalence.

In summary, in this dissertation we develop new tools and framework to understand the effect of wheel slip in the control of a WMR and show how the presented approach allows solutions in various important WMR applications.

7.2 Future Work

This dissertation present the results of initial investigation into the control of a WMR subject to wheel slip and opens opportunities for further research in several directions.

First, the model of the WMR subject to wheel slip and the designed controllers need to be verified in experiments. Several research groups have been looking into techniques to measure slips in real-time and developing various techniques to estimate slips and traction forces [16][17][18]. Their research will need to be synergistically combined with the proposed control techniques in this dissertation to develop realistic slip-based controllers for WMR in the future. Such robust control methods will be useful in many realistic applications.

Second, from the optimal control perspective, new optimality criteria can be formulated considering wheel slip. The optimal control problems for a WMR can be represented in the light of wheel slip, which relaxes kinematic constraints. For example, Dubin's curve is an optimization problem for a WMR without slip, where the goal is to find a curve of minimum distance that connects two given configurations. Once slip is introduced, the problem becomes finding a new Dubin's curve in the light of slip and its corresponding traction force, which is nonlinearly dependent on slip, speed of the WMR and friction coefficient. More generally, if a kinematic constraint is possible to be relaxed in a general dynamic system, the optimization problem for the original system becomes a new problem.

Third, vehicle control is a major application where wheel slip is involved. In platoon control of automated highway systems, for example, safety is important, which is guaranteed by preserving proper distances between vehicles. However, when braking occurs for the leader vehicle, each following vehicle in the platoon need to deal with slip and time delay while maintaining proper distance from others. In this case, slip based

control could play an important role in managing time delay and maintaining distance from others.

REFERENCES

[1] Yangquan Chen and Zhongmin Wang, "Formation Control: a review and a new consideration", *IEEE International Conference on Intelligent Robots and Systems*, 2005, pp. 3181-3186.

[2] Sarkar N., Yun X., "Control of mechanical systems with rolling constraints: Application to the dynamic control of mobile robots", *Int. Journal of Robotics Research*, Vol. 31, 1994, pp. 55-69.

[3] Motte I., Campion I., "A slow manifold approach for the control of mobile robots not satisfying the kinematic constraints", *IEEE Trans. on Robotics and Automation*, Vol. 16, No. 6, 2000, pp. 875-880.

[4] Lin W.-S., Chang L.-H., Yang P.-C., "Adaptive critic anti-slip control of wheeled autonomous robot", Control Theory & Applications, IET, Vol. 1, Issue 1, 2007, pp. 51-57.

[5] Tarokh M., McDermott G.J., "Kinematics modeling and analyses of articulated rover", *IEEE Trans. on Robotics*, Vol. 21, No.4, 2005, pp. 539-553.

[6] Dixon W.E., Dawson D.M., Zergeroglu E., "Robust control of a mobile robot system with kinematic disturbance", *IEEE Int. Conference on Control Applications*, 2000, pp. 437-442.

[7] Balakrishna R. and Ghosal A., "Modeling of slip for wheeled mobile robot", *IEEE Trans. on Robotics and Automation*, Vol. 11, No. 1, 1995, pp. 126-132.

[8] Jung S., Hsia T.C., "Explicit lateral force control of an autonomous mobile robot with slip", *IEEE/RSJ Int. Conf. on Intelligent Robots and Systems*, IROS 2005, pp. 388-393.

[9] Stonier D., Hyoung C. Se-, Sung-Lok C., Kuppuswamy N.S., Jong-Hwan K., "Nonlinear slip dynamics for an omni-wheel mobile robot platform", *IEEE Int. Conf. on Robotics and Automation*, 2007, pp. 2367-2372.

[10] Jeren Ploeg, Hanno E. Schouten and Henk Nijmeijer, "Control Design for a Mobile Robot Including Tire Behavior", *2008 IEEE Intelligent Vehicles Symposium*, Eindhoven, The Netherlands, June 4-6, 2008, pp. 240-245.

[11] Lagerberg A. and Egardt B., "Backlash estimation with application to automotive powertrains", *IEEE Trans. on Control Systems Technology*, 15(3), 2007, pp. 483-493.

[12] Verma R., Vecchio D., and Fathy H., "Development of a scaled vehicle with longitudinal dynamics of an HMMWV for an ITS testbed", *IEEE/ASME Trans.on Mechatronics*, 13(1), 2008, pp. 46-57.

[13] Kyung-Ho B., "Development of dynamics modeling in the vehicle simulator for road safety analysis", *Annual Conference SICE07*, 2007, pp. 649-653.

[14] Der-Chen L. & Wen-Ching C., “Control design for vehicle's lateral dynamics”, *IEEE Int. Conf. on Systems, Man and Cybernetics, ICSMC '06*, 3, pp. 2081-2086.

[15] N. Sidek, “Dynamic Modeling and Control of Nonholonomic Wheeled Mobile Robot Subjected to Wheel Slip”, PhD Thesis, Vanderbilt University, USA, 2008.

[16] Ward C.C., Iagnemma K., “Model-based wheel slip detection for outdoor mobile robots”, *IEEE Int. Conf. on Robotics and Automation*, 2007, pp. 2724-2729.

[17] Angelova A., Matthies L., Helmick D.M., Sibley G., Perona P., “Learning to predict slip for ground robots”, *Proc. of IEEE Int. Conf. on Robotics and Automation*, 2006, pp. 3324-3331.

[18] Seyr M., Jakubek S., “Proprioceptive navigation, slip Estimation and slip control for autonomous wheeled mobile robot”, *IEEE Conf. on Robotics,Automation and Mechatronics*, Dec. 2006, pp. 1-6.

[19] Germann M., Wurtenberger A. & Daiss A., “Monitoring of the friction coefficient between tyre and road surface”, *Proc. of the Third IEEE Conf. on Control Applications*, 1, Aug. 1994, pp. 613-618.

[20] Li L., Wang F.Y., “Integrated longitudinal and lateral tire/road friction modeling and monitoring for vehicle motion control”, *IEEE Trans. on Intelligent Transportation Sys*, **7**(**1**), 2006, pp. 1-19.

[21] Bakker E., Nyborg L., Pacejka H.B., “Tire modeling for the use of the vehicle dynamics studies”, *SAE paper*, 1987, 870421.

[22] R. Fierro and F. L. Lewis, “Control of a Nonholonomic Mobile Robot: Backstepping Kinematics into Dynamics”, Journal of Robotics Systems, 14(3), 1997, pp. 149-163.

[23] Guldner, J and Utkin, V.I., “Stabilization of non-holonomic robots using Lyapunov functions for navigation and sliding mode control”, *Proc. of IEEE International Conference on Decision and Control*, vol. 3, Dec. 1994, pp. 2967-2972.

[24] Jong-Min Yang and Jong-Hwan Kim, “Sliding mode control for trajectory tracking of nonholonomic wheeled mobile robots”, *IEEE Trans. on Robotics and Automation*, vol. 15, Issue 3, 1999, pp. 578-587.

[25] Khac Duc Do, Zhong-Ping Jiang and Jie Pan, “A Global Output-Feedback Controller for Simultaneous Tracking and Stabilization of Unicycle-Type Mobile Robots”, *IEEE Trans. on Robotics and Automation*, vol. 20, No. 3, 2004, pp. 589-594.

[26] Daliang Liu, Hanxu Sun and Qingxuan Jia, “A family of spherical mobile robot: Driving ahead motion control by feedback linearization”, *IEEE International Symposium on Systems and Control in Aerospace and Astronautics*, Dec. 2008, pp. 1-6.

[27] Yun X, Yamamoto Y., “Internal dynamics of a wheeled mobile robot”, *IEEE/RSJ Int. Conf. on Intelligent Robots and Systems*, Yokohama Japan, 1993, pp. 1288-1294.

[28] Kumar V., Wellman P., Krovi V., Appl. No.: 239,951, Filed: May 9, 1994, Granted: May 7, 1996, Adaptive mobility system, United States Patent 5,513,716.

[29] Sergio M. Savaresi, Mara Tanelli and Carlo Cantoni, “Mixed Slip-Deceleration Control in Automotive Braking Systems”, *J. of Dynamic Systems, Measurement, and Control*, Vol. 129, Issue 1, 2007, pp. 20-31.

[30] Tor A. Johansen, Idar Petersen, Jens Kalkkuhl and Jens Ludemann, “Gain-Scheduled Wheel Slip Control in Automotive Brake Systems”, *IEEE Trans. on Control Systems Technology*, vol. 11, No. 6, 2003, pp. 799-811.

[31] H. Yu and U. Ozguner, “Extremum-Seeking Control Stragegy for ABS System with Time Delay”, *Proceedings of American Control Conference*, vol. 5, May. 2002, pp. 3753-3758.

[32] S. Drakunov, U. Ozguner, P. Dix and B. Ashrafi, “ABS Control Using Optimum Search via Sliding Modes”, *IEEE Trans. on Control Systems Technology*, vol. 3, No. 1, Mar. 1995, pp. 79-85.

[33] I. Haskara, U. Ozguner and J. Winkelman, “Wheel Slip Control for Antispin Acceleration via Dynamic Spark Advance”, *Control Engineering Practice*, vol. 8, 2000, pp. 1135-1148

[34] Shou-Tao Peng, “On One Approach to Constraining the Combined Wheel Slip in the Autonomous Control of a 4WS4WD Vehicle”, *IEEE Trans. on Control System Technology*, Vol. 15, No. 1, 2007, pp. 168-175.

[35] Matteo Amodeo, Antonella Ferrara, Riccardo Terzaghi and Claudio Vecchio, “Wheel Slip Control via Second-Order Sliding-Mode Generation”, *IEEE Conference on Decision and Control*, Dec. 2007, pp. 3889-3894.

[36] Takanori Fukao, Hiroshi Nakagawa and norihiko Adachi, “Adaptive Tracking Control of a Nonholonomic Mobile Robot”, *IEEE Trans. on Robotics and Automation*, vol. 16, No. 5, 2000, pp. 609-615.

[37] Zhong-ping Jiang and Henk Nijmeijer, “Tracking Control of Mobile Robots: A Case Study in Backstepping”, *Automatica*, vol. 33, No. 7, 1997, pp. 1393-1399.

[38] Mahmut Reyhanoglu, “Exponential Stabilization of an Underactuated Autonomous Surface Vessel”, *Automatica*, Vol. 33, No. 12, 1997, pp. 2249-2254.

[39] Frederic Mazenc, Kristin Pettersen and Henk Nijmeijer, “Global Uniform Asymptotic Stabilization of an Underactuated Surface Vessel”, *IEEE Trans. on Automatic Control*, Vol. 47, No. 10, 2002, pp.

1759-1762.

[40] Dong, Wenjie and Guo, Yi, “Global Time-Varying Stabilization of Underactuated Surface Vessel”, *IEEE Trans. on Automatic Control*, Vol. 50, No. 6, 2005, pp. 859-864.

[41] Jawhar Ghommam, Faical Mnif, Abderraouf Benali and Nabil Derbel, “Asymptotic Backstepping Stabilization of an Underactuated Surface Vessel”, *IEEE Trans. on Control Systems Technology*, Vol. 14, No. 6, 2006, pp. 1150-1157.

[42] A. Behal, D. M. Dawson, W. E. Dixon and Y. Fang, “Tracking and Regulation Control of an Underactuated Surface Vessel With Nonintegrable Dynamics”, *IEEE Trans. on Automatic Control*, Vol. 47, No. 3, 2002, pp. 495-500.

[43] Slotine, J.-J. E. And W. Li, *Applied nonlinear Control*, Prentice-Hall, Englewood Cliffs, NJ,1991.

[44] Yu Tian and Nilanjan Sarkar, “Near-Optimal Autonomous Pursuit Evasion for Nonholonomic Wheeled Mobile Robot Subject to Wheel Slip”, *IEEE International Conference on Robotics and Automation*, Anchorage, USA, May 2010, accepted.

[45] Dubins L.E., “On curves of minimal length with a constraint on average curvature, and with prescribed initial and terminal positions and tangents”, *American Journal of Mathematics*, Vol. 79, 1957, pp. 497-516.

[46] Desai, J.P., Ostrowski, J.P., Kumar, V., “Modeling and control of formations of nonholonomic mobile robots”, *IEEE Trans. on Robotics and Automation*, vol. 17, issue 6, 2001, pp. 905 - 908.

[47] Travis Dierks and S. Jagannathan, “Control of Nonholonomic Mobile Robot Formations: Backstepping Kinematics into Dynamics”, *IEEE International Conference on Control Applications*, 2007, pp. 94-99.

[48] S. A. Panimadai Ramaswamy and S. N. Balakrishnan, “Formation Control of Car-Like Mobile Robots: A Lyapunov Function Based Approach”, *2008 American Control Conference*, pp. 657-662.

[49] Ian L. Dryden and Kanti V. Mardia, *Statistical Shape Analysis*, John Wiley & Sons, West Sussex, England, 1998.

[50] V. Isler, S. Kannan and S. Khanna, “Ramdomized pursuit-evasion in a polygonal environment”, *IEEE Trans. on Robotics*, Vol. 21, Issue 5, 2005, pp. 875-884.

[51] P. Kachroo, S.A. Shedied, J.S. Bay, H. Vanlandingham, “Dynamic programming solution for a class of pursuit evasion problems: the herding problem”, *IEEE Trans. on System, Man, and Cybernetics, Part C: Applications and Reviews*, Vol. 31, Issue 1, 2001, pp. 35-41.

[52] K. D. Pham, S. Lacy and L. Robertson, “Multi-cumulant and pareto strategies for stochastic multi-player pursuit-evasion”, *Proceedings of American Control Conference*, Jun. 2008, pp. 5009-5015.

[53] J. Sprinkle, J.M. Eklund, H.J. Kim and S. Sastry, “Encoding aerial pursuit/evasion games with fixed wing aircraft into a nonlinear model predictive tracking controller”, *IEEE Conference on Decision and Control*, Vol. 3, Dec. 2004, pp. 2609-2614.

[54] D. Li and J.B. Cruz, “Graph-based strategies for multi-player pursuit evasion games”, *IEEE Conference on Decision and Control*, Dec. 2007, pp. 4063-4068.

[55] S. H. Lim, T. Furukawa, G. Dissanayake and H.F. Durrant-Whyte, “A time-optimal control strategy for pursuit-evasiongames problems”, *IEEE International Conference on Robotics and Automation*, Vol. 4, 2004, pp. 3962-3967.

[56] R. Isaacs, *Differential Games: a mathematical theory with applications to warfare and pursuit, control and optimization*. John Wiley and Sons, New York, 1965.

[57] Ian Michael Mitchell, “Application of Level Set Methods to Control and Reachability Problems in Continuous and Hybrid Systems”, PhD Thesis, Stanford University, USA, 2002.

[58] A. W. Merz, The game of two identical cars. *Journal of Optimization Theory and Applications.* 9(5), 1972, pp. 324-343.

[59] Ian M. Mitchell and Jeremy A. Templeton, “A Toolbox of Hamilton-Jacobi Solvers for Analysis of Nondeterministic Continuous and Hybrid Systems”, *Hybrid Systems: Computation and Control*, Mar. 2005, pp. 480-494.

[60] Morten Breivik and Thor I. Fossen, “Guidance Laws for Planar Motion Control”, *IEEE Conference on Decision and Control*, Cancun, Mexico, Dec. 2008, pp. 570-577.

[61] Yu Tian, Naim Sidek and Nilanjan Sarkar, “Tracking Control for Nonholonomic Wheeled Mobile Robot with Wheel Slip Dynamics”, *ASME Dynamic System and Control Conference*, Hollywood, USA, Oct. 2009.

[62] Ian Mitchell, Alexandre Bayen and Claire Tomlin, “Validating a Hamilton-Jacobi Approximation to Hybrid System Reachable Sets”, *Hybrid Systems Computation and Control*, Apr. 2001, pp. 418-432.

[63] Communication with Dr. Ian Mitchelle, Computer Science Department, University of British Columbia, Canada.

Appendix:

$$M^{-1} = \begin{bmatrix} A & -bB & bB \\ -bB & E-bD & E+bD \\ bB & E+bD & E-bD \end{bmatrix} = \begin{bmatrix} \frac{md^2+I}{mI} & -\frac{db}{I} & \frac{db}{I} \\ -\frac{db}{I} & \frac{mb^2+I}{mI} & -\frac{mb^2-I}{mI} \\ \frac{db}{I} & -\frac{mb^2-I}{mI} & \frac{mb^2+I}{mI} \end{bmatrix}$$

where $A = \frac{md^2+I}{mI}$, $B = \frac{d}{I}$, $D = -\frac{b}{I}$, $E = \frac{1}{m}$.